HHS Public Access

Author manuscript

Cell Rep. Author manuscript; available in PMC 2022 December 28.

Published in final edited form as:

Cell Rep. 2022 November 08; 41(6): 111610. doi:10.1016/j.celrep.2022.111610.

Sex differences in resilience to ferroptosis underlie sexual dimorphism in kidney injury and repair

Shintaro Ide[1,7], **Kana Ide**[1,7], **Koki Abe**[1,7], **Yoshihiko Kobayashi**[2,6], **Hiroki Kitai**[1], **Jennifer McKey**[2], **Sarah A. Strausser**[1], **Lori L. O'Brien**[3], **Aleksandra Tata**[2], **Purushothama Rao Tata**[2,4,5], **Tomokazu Souma**[1,4,8,*]

[1]Division of Nephrology, Department of Medicine, Duke University School of Medicine, Durham, NC 27710, USA

[2]Department of Cell Biology, Duke University School of Medicine, Durham, NC 27710, USA

[3]Department of Cell Biology and Physiology, University of North Carolina at Chapel Hill, Chapel Hill, NC 27599, USA

[4]Duke Regeneration Center, Duke University School of Medicine, Durham, NC 27710, USA

[5]Duke Cancer Institute, Duke University School of Medicine, Durham, NC 27710, USA

[6]Present address: Institute for Life and Medical Sciences, Kyoto University, Kyoto 606-8397, Japan

[7]These authors contributed equally

[8]Lead contact

Abstract

In both humans and mice, repair of acute kidney injury is worse in males than in females. Here, we provide evidence that this sexual dimorphism results from sex differences in ferroptosis, an iron-dependent, lipid-peroxidation-driven regulated cell death. Using genetic and single-cell transcriptomic approaches in mice, we report that female sex confers striking protection against ferroptosis, which was experimentally induced in proximal tubular (PT) cells by deleting glutathione peroxidase 4 (*Gpx4*). Single-cell transcriptomic analyses further identify the NFE2-related factor 2 (NRF2) antioxidant protective pathway as a female resilience mechanism against ferroptosis. Genetic inhibition and pharmacological activation studies show that NRF2 controls PT cell fate and plasticity by regulating ferroptosis. Importantly, pharmacological NRF2 activation

*Correspondence: tomokazu.souma@duke.edu.

AUTHOR CONTRIBUTIONS

S.I., K.I., K.A., H.K., J.M., S.A.S., and T.S. performed experiments; Y.K., S.I., P.R.T., and T.S. designed the single-cell transcriptomics experiments and analyzed the data; A.T., and P.R.T. contributed new protocols/reagents/analytical tools; S.I., K.I., K.A., L.L.O., and T.S. analyzed the data; T.S., S.I., K.I., K.A., H.K., L.L.O., and P.R.T. wrote the manuscript. T.S. conceived and supervised the study. All authors read, commented, and approved the manuscript.

DECLARATION OF INTERESTS

The authors declare no competing interests.

SUPPLEMENTAL INFORMATION

Supplemental information can be found online at https://doi.org/10.1016/j.celrep.2022.111610.

protects male PT cells from ferroptosis and improves cellular plasticity as in females. Our data highlight NRF2 as a potential therapeutic target to prevent failed renal repair after acute kidney injury in both sexes by modulating cellular plasticity.

In brief

Repair of acute kidney injury is worse in males than in females. Ide et al. report that this sexual dimorphism results from sex differences in ferroptosis. Single-cell transcriptomics identifies NRF2 as a female resilience mechanism and regulator of cellular plasticity. Targeting NRF2 holds the promise to improve acute kidney injury outcomes.

Graphical Abstract

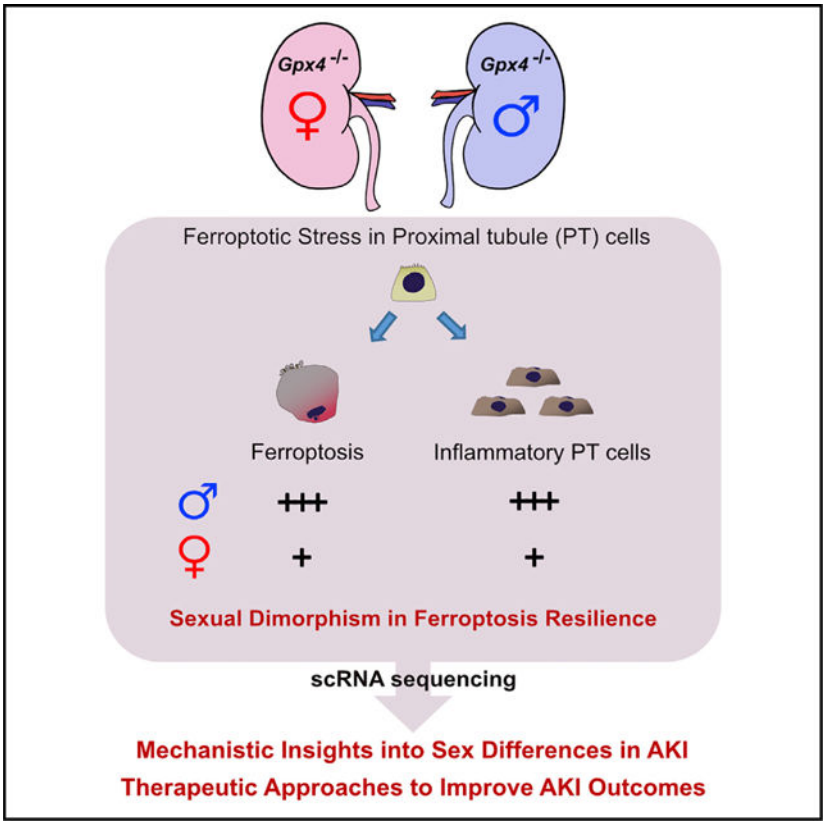

INTRODUCTION

Acute kidney injury (AKI) is a major health problem, afflicting 1.2 million hospitalized patients annually in the US (Chawla et al., 2014; Lewington et al., 2013). Up to half of these patients fail to undergo renal repair and progress to chronic kidney disease (CKD), a condition associated with significantly increased morbidity and mortality (Chawla et al., 2014; Ferenbach and Bonventre, 2015; Goldstein et al., 2013). Kidney damage is also common in COVID-19 disease, with 30%–50% of hospitalized patients manifesting AKI and some survivors progressively losing kidney function (Bowe et al., 2021; Nadim et al., 2020). To interrupt these devastating disease outcomes, we urgently need new

therapeutic approaches. One clue to achieving this goal is the sexual dimorphism seen in kidney injury and repair processes (Bairey Merz et al., 2019; Mauvais-Jarvis et al., 2020). Increasing evidence shows that men are disproportionately and more severely affected by AKI than women (Bagshaw et al., 2005; Hsu et al., 2013; Neugarten and Golestaneh, 2018; Neugarten et al., 2018), including COVID-19-associated AKI (Fisher et al., 2020; Nadim et al., 2020). In humans, male kidneys transplanted to premenopausal women are protected from ischemia-reperfusion injury (IRI), suggesting a protective effect of the female hormonal environment (Aufhauser et al., 2016). Indeed, AKI is less prevalent in transfeminine individuals under-going gender-affirming hormone therapy compared with those not receiving hormone therapy (Eckenrode et al., 2022). Preclinical rodent studies have also repeatedly found that female kidneys are resistant to acute and chronic injuries, and this is partly dependent on sex hormonal environment (Bairey Merz et al., 2019; Harris and Zhang, 2020). Together, these observations suggest that elucidating sex-dependent molecular mechanisms underlying resilience to injury will point to new therapeutic approaches.

Ferroptosis is a distinct, non-apoptotic form of regulated cell death triggered by the pathologic accumulation of toxic membrane lipid peroxides in an iron-dependent manner (Dixon et al., 2012; Jiang et al., 2021; Yang et al., 2014; Zou and Schreiber, 2020). Cellular sensitivity and resistance to ferroptosis are primarily determined by transcriptional and metabolic cell states under complex interactions between cells and their microenvironment (Jiang et al., 2021; Zou and Schreiber, 2020). Importantly, ferroptosis is emerging as a critical driver of acute and chronic kidney diseases in mice and humans (Balzer et al., 2022; Friedmann Angeli et al., 2014; Guan et al., 2021; Ide et al., 2021; Li et al., 2021; Linkermann et al., 2014; Maremonti et al., 2022; Muller et al., 2017; Wenzel et al., 2017). For example, insufficient activity of glutathione peroxidase 4 (GPX4), the central defense pathway against ferroptosis, causes an imbalance in the generation and elimination of toxic lipid peroxides and increases ferroptotic stress in proximal tubular (PT) epithelial cells, triggering ferroptotic cell death and promoting maladaptive renal repair (Friedmann Angeli et al., 2014; Ide et al., 2021; Ingold et al., 2018; Maremonti et al., 2022). Moreover, estradiol has been shown to affect the cellular redox state in humans and to prevent ferroptosis in cell culture (Bellanti et al., 2013; Mishima et al., 2020). These observations raise the intriguing idea that ferroptosis is a sex-dependent regulated cell death process in the kidney.

Here, using complementary mouse genetic and single-cell transcriptomic approaches, we have uncovered a protective role of female sex against ferroptosis in the kidney. In addition, our single-cell transcriptomics studies reveal that NF-E2-related factor 2 (NRF2) (Yamamoto et al., 2018) is a potential regulator of ferroptotic resilience in females. Our genetic loss-of-function and pharmacological gain-of-function studies show that NRF2 functions as a molecular “rheostat,” modulating the ferroptosis sensitivity of PT cells *in vivo*, and provide a molecular explanation for female resilience against ferroptosis. Taken together, our results raise the possibility that NRF2 can be therapeutically harnessed to inhibit ferroptosis in kidneys and thereby improve renal repair and regeneration after injury in both sexes.

RESULTS

Female sex protects renal tubular epithelial cells from ferroptosis

PT cells are among the most severely affected targets of acute ischemic and toxic injuries and are vulnerable to ferroptotic stress and ferroptosis (Ferenbach and Bonventre, 2015; Friedmann Angeli et al., 2014; Guan et al., 2021; Ide and Souma, 2022; Ide et al., 2021; Linkermann et al., 2014). To identify potential sex differences in the ferroptotic process in kidneys, we first generated a mouse line (*Pax8rtTA*; *tetO-Cre*; *Gpx4*$^{fl/fl}$, herein *Gpx4* conditional knockout [cKO]) in which ferroptotic stress and ferroptosis can be selectively induced in adult renal tubular epithelial cells in a doxycycline-inducible manner (Figure 1A). Doxycycline feeding robustly induced Cre-mediated deletion of exons 2–4 of the *Gpx4* allele, including the region encoding the catalytically active selenocysteine site of the *GPX4* protein. We confirmed the consistent deletion of *Gpx4* at mRNA and protein levels in both males and females (Figures S1A and S1B).

In male, but not female, mice, *Gpx4* deletion caused tubular epithelial injury and reduced kidney function, marked by doubling of serum creatinine levels on day 10 (Figures 1B and 1C; Figure S1E). *Gpx4*-deleted male kidneys also exhibited significant accumulation of 4-hydroxynonenal (4-HNE), a highly reactive and pathogenic molecule generated during lipid peroxidation (Figures S1C and S1D). We observed robust induction of tubular injury markers, such as kidney injury molecule-1 (KIM1; encoded by *Havcr1*) (Ichimura et al., 2008), cytokeratin 20 (*Krt20*) (Liu et al., 2017), and neutrophil gelatinase-associated lipocalin (NGAL; encoded by *Lcn2*) (Paragas et al., 2011) in male *Gpx4* cKO kidneys (Figures 1D and 1E; Figure S1F). Moreover, these kidneys show deposition of extracellular matrix components such as collagen 1a1 and increased numbers of renal F4/80^{+} macrophages (Figures 1D and 1E; Figure S1F), which are characteristic of failed repair after AKI (Ferenbach and Bonventre, 2015; Ide et al., 2021).

We assessed cell death using the terminal deoxynucleotidyl transferase-mediated dUTP nick end labeling (TUNEL) assay, which detects ferroptotic cell death in *Gpx4*-deleted tissues (Friedmann Angeli et al., 2014; Grasl-Kraupp et al., 1995; Ide and Souma, 2022; Ide et al., 2021; Maremonti et al., 2022). Consistent with the known central role of GPX4 in preventing ferroptosis (Friedmann Angeli et al., 2014; Ingold et al., 2018; Yang et al., 2014), genetic deletion of *Gpx4* results in increased TUNEL^{+} tubular epithelial cells in male, but not female, cKO kidneys at this time (Figures 1F and 1G). The male cKO kidneys were negative for cleaved caspase 3, providing further evidence that ferroptosis is distinct from apoptosis (Figure S1G) (Friedmann Angeli et al., 2014; Ingold et al., 2018). Strikingly, as indicated, female *Gpx4* cKO mice did not show increases in tubular injury markers (*Kim1*, *Krt20*, and *Lcn2*), lipid peroxidation (4-HNE), collagen production, or TUNEL^{+} cells. Their kidney function also did not change from baseline (Figures 1B and 1D–1G; Figures S1C–S1F). In summary, our comparative analyses of male and female *Gpx4* cKO kidneys demonstrate that female kidneys are markedly resistant to *Gpx4* deletion-induced acute kidney damage and ferroptosis.

Intact ovarian function is essential for female ferroptosis resilience

In mammals, sex differences in biological and pathological processes arise from an intricate network of factors including developmental pathways, products of the neuroendocrine axis, and genes located on sex chromosomes (Bairey Merz et al., 2019; Mauvais-Jarvis et al., 2020). To investigate the potential role of the sex hormonal environment on female resistance to renal tubular ferroptosis, we evaluated the female kidneys from ovariectomized (OVX) and sham-operated (hormonally intact) *Gpx4* cKO mice and their littermates (Figure 2A). As expected, *Gpx4*-deficient kidneys from sham-operated mice did not show signs of kidney injury, including no elevation of serum creatinine, induction of renal tubular injury markers (KIM1 and KRT20), or increased cell death ($TUNEL^+$ cells) (Figure 2; Figure S2). However, ovariectomy attenuated the female protection of *Gpx4* cKO mice. Ovariectomy (OVX) worsened the kidney function of *Gpx4*-deficient female kidneys (Figure 2B) and increased expressions of KIM1 and 4-HNE and the number of $TUNEL^+$ cells (Figures 2C–2G; Figure S2), although the magnitude of injury was still not as severe as seen in male *Gp×4* cKO kidneys. Collectively, our data demonstrate that female sex confers resilience to ferroptosis and ferroptotic stress in kidneys through ovarian-dependent and -independent mechanisms.

scRNA sequencing identifies inflammatory PT cells in male Gpx4-deficient kidneys

Next, we utilized single-cell RNA sequencing (scRNA-seq) to uncover additional mechanisms by which female kidneys are resistant to ferroptotic stress *in vivo* and decipher cellular states that accompany following *GPX4* loss of function. Kidneys of male and female Gpx4 cKO mice as well as their littermates were harvested for scRNA-seq analysis at 10 days after initiating doxycycline feeding, a time when we observed significant and most extensive female protection against ferroptosis (Figure 3A). Data from 8 independent kidneys were filtered to eliminate potential doublets and low-quality cells, followed by integration to minimize potential batch effects while maintaining biological variables (30,927 cells; Figure 3B; Figure S3A) (Hafemeister and Satija, 2019; Hao et al., 2021). We then performed unsupervised clustering analysis of the integrated dataset. Uniform manifold approximation and projection (UMAP) resolved all major cell types in the kidneys (Figure 3B). The cellular identity of each cluster was determined based on the known cell-type-specific markers, as we previously demonstrated (Figure S3B) (Ide et al., 2021).

We identified a unique cluster of cells that are mostly derived from male *Gpx4* cKO kidneys (damage-associated PT [DA-PT] cells in Figure 3B). The transcriptional signature of the cells in this cluster resembles that of recently described inflammatory PT cells (Figures S3C and S3D), a pathologic cell state associated with maladaptive and failed renal repair and characterized by expression of Sry-box 9 (SOX9) and vascular cell adhesion molecule 1 (VCAM1) (Gerhardt et al., 2021; Ide et al., 2021; Kirita et al., 2020). Inflammatory PT cells express high levels of injury and regeneration-related genes but reduced expression of mature PT cell genes as observed previously after ischemic and toxic injuries (Figure 3C) (Gerhardt et al., 2021; Ide et al., 2021; Kirita et al., 2020; Lu et al., 2021). Our computational inference using Monocle 3 (Cao et al., 2019) suggests that inflammatory PT cells are derived from mature PT cells in male *Gpx4* KO mice, as in IRI models (Gerhardt et al., 2021; Ide et al., 2021; Kirita et al., 2020) (Figure 3D). Immunofluorescence and qRT-

PCR analyses validated the accumulation of $SOX9^{+}VCAM1^{+}$ cells in male *Gpx4*-deleted kidneys but not in other conditions (Figures 3E and 3F). Interestingly, we also observed the accumulation of $SOX9^{+}VCAM1^{+}$ PT cells in ovariectomized *Gpx4*-deficient female kidneys, whereas none were observed in *Gpx4*-deficient female kidneys of hormonally intact controls (Figures S2F and S2G). This result suggests that an intact female hormonal environment is a key determinant of PT cell fate. Together with our recent report (Ide et al., 2021), our results substantiate our model that ferroptotic stress governs PT cell plasticity and cell-fate decision in a sex-dependent manner.

scRNA-seq identifies potential molecular pathways underlying female resilience to ferroptosis

We hypothesized that female resilience against ferroptosis is controlled by gene sets that are highly expressed in female PT cells compared with male, both at baseline and after *Gpx4* deletion. We identified 128 genes that fall into this category. Their analysis using "Enrichr" (Kuleshov et al., 2016) identified the NRF2 antioxidant cellular defense pathway (Yamamoto et al., 2018) as a top candidate protective pathway, among others (Figures 4A–4C). To further dissect the transcriptional regulatory networks underlying sex-dependent responses to ferroptotic stress, we performed additional computational analyses using single-cell regulatory network inference and clustering (SCENIC), which infers candidate transcription factors governing cell states across conditions by linking cis-regulatory sequence information with the co-expression pattern of transcription factors and target genes in each cell (Figure 4D) (Aibar et al., 2017). We applied SCENIC to a total of 15,416 PT cells from all four conditions, allowing us to cluster each cell based on its gene regulatory network activity or regulons. Our analyses identified distinct patterns of regulatory nodes that are active in PT cells in an unbiased way. For example, we noticed that some regulons are highly active in both male and female *Gpx4* KO PT cells (e.g., *Atf4*, *Xbp1*, *Cebpb*), but others are differentially enriched in one or other sex (Figure 4D; Figure S4).

The SCENIC analysis again identified NRF2 as the highly over-represented regulon enriched in female PT cells from both *Gpx4*-intact and KO mice (Figure 4D). UMAP representation of NRF2 regulon activity clearly shows much higher activity in female compared with male PT cells. Moreover, the number of cells with high NRF2 regulon activity was increased by *Gpx4* deletion in both sexes but, again, to a higher level in females (Figure 4D). These two independent analyses suggest that NRF2 signaling is a potential pathway that confers female resilience to ferroptotic stress. In support of our finding, higher female NRF2 activity than male at baseline was observed in mouse and human livers (Liu et al., 2021; Rooney et al., 2018), suggesting that the role of NRF2 in conferring ferroptosis resilience in females may extend to other organ systems.

Nrf2-target genes are differentially regulated in PT cells between sexes

Among the differentially expressed genes, *Gsta4*, *Gstm1*, and *Mgst1* are of particular interest due to their known functions in cellular redox regulation (Figures S5 and S6). The glutathione transferases encoded by these genes are crucial for protecting cells against electrophiles and oxidative stress, and they are effectors of NRF2 signaling (Hayes et al., 2005; Yamamoto et al., 2018). GSTA4 is the major enzyme that detoxifies

4-HNE and is protective against renal inflammation and fibrosis in a ureteral obstruction model (Liangetal.,2012). *GSTM1*-null variants are highly prevalent in the general human population, ranging from 25% to 50%, and increase the risk of heart failure and end-stage kidney diseases (Gigliotti et al., 2020; Tin et al., 2017). MGST1 protects human pancreatic cancer cell organoids from ferroptosis (Kuang et al., 2021). We confirmed the NRF2-mediated regulation of these genes by applying a potent pharmacological inducer of NRF2 (1-[2-cyano-3,12-dioxooleana-1,9(11)-dien-28-oyl] imidazole [CDDO-Im]) (Nezu et al., 2017; Yates et al., 2007). These genes were significantly induced by CDDO-Im in mouse kidneys but not in *Nrf2*-null mouse embryonic fibroblasts (MEFs) (Figure S7).

UMAP representation of each gene clearly shows the higher expression in female PT cells compared with males (Figures S6A, S6D, and S6G). In support of our computational analyses, studies using qRT-PCR and RNAScope *in situ* hybridization with a validation cohort of mice confirmed the higher expression of these genes in lotus-tetragonolobus lectin (LTL)-expressing female PT cells than in male PT cells (Figure S6). Our validation studies also confirmed the female-enriched expression pattern of other predicted female resilience genes, which have roles for cysteine synthesis (cystathionine gammalyase [*Cth*]) (Zhu et al., 2019) and inactivation of highly reactive lipid aldehydes such as 4-HNE (carbonyl reductase 1 [*Cbr1*]) (Oppermann, 2007) (Figures S5B and S5C).

To test the effects of male and female sex hormones on these glutathione metabolic genes, we performed OVX in females and orchiectomy (ORX) in males (Figure S8A). While OVX did not alter the expression levels, we observed a robust induction of these genes in male kidneys from orchiectomized mice (Figures S8B–S8D). These data suggest that a low-testosterone female microenvironment underlies the sexual dimorphism of glutathione metabolic gene expression.

Collectively, our data suggest two significant conclusions: that sex differences in NRF2 activity underlie the resilience of female PT cells to ferroptosis and that promoting NRF2 expression levels in male PT cells may confer resistance to ferroptosis as in females.

Genetic loss of Nrf2 in inflammatory PT cells prevents renal repair after IRI

While the role of NRF2 in ferroptosis resistance has been postulated from studies using cancer cells (Kuang et al., 2021; Sun et al., 2016; Takahashi et al., 2020), it has been underappreciated as to how NRF2 regulates ferroptotic stress and governs epithelial cell fate during tissue repair *in vivo*. We hypothesized that *Nrf2* gene activity acts as a “molecular rheostat” to control PT cell fate under high ferroptotic stress such as after IRI. We tested this hypothesis using combined genetic loss-of-function, pharmacological inhibitor, and fate-mapping studies (Figures 5A and 6A). We generated a mouse line in which *Nrf2* can be selectively and conditionally deleted using a CreERT2 allele of *Sox9*, a gene that is highly induced in damaged and repairing PT cells after IRI (Ide et al., 2021; Kang et al., 2016; Kumar et al., 2015). In this mouse line, tamoxifen administration deletes exon 5 (encoding the DNA-binding domain) of the *Nrf2* allele in *Sox9*-lineage cells ($Sox9^{CreERT2}$; $Nrf2^{flox/flox}$; herein, *Nrf2* cKO) after IRI (Figure 5A). PT cells of the contralateral uninjured kidney (CLK) are not targeted by this Cre line as the *Sox9* gene is only induced in PT cells after renal damage (Ide et al., 2021; Kumar et al., 2015).

We subjected *Nrf2* cKO mice and Cre-negative control littermates (*Nrf2*$^{flox/flox}$) to mild renal ischemic stress (ischemic time: 20 min). All mice received tamoxifen to eliminate confounding by tamoxifen injection (Figure 5A). In this condition, the kidneys of control mice successfully repair on day 21 after IRI, as previously reported (Ide et al., 2021). *Nrf2*-deleted kidneys exposed to IRI robustly expressed KIM1 and showed a higher number of SOX9^{+}VCAM1^{+} inflammatory PT cells on day 21 after IRI compared with *Nrf2*-intact IRI kidneys (Figures 5B–5E; see CLK data in Figure S9B). *Nrf2* deletion also increased ferroptotic stress markers (4-HNE and acyl-CoA synthetase long-chain family member 4 [ACSL4]) and the number of TUNEL^{+} cells (Figures 5F–5I; see CLK data in Figures S9B and S9C), and these pathological changes were associated with an increase of F4/80^{+} macrophages and collagen 1 deposition (Figures S9D and S9E). By contrast, *Nrf2*-intact control littermate kidneys that underwent the same ischemic stress did not show these pathological changes, indicating that these kidneys successfully repaired after IRI (control IRI; Figure 5; Figure S9). Collectively, these data indicate that genetic deletion of *Nrf2* in *Sox9*-lineage cells is sufficient to prevent normal renal repair after mild ischemic injury and to induce failed renal repair phenotypes.

Pharmacological inhibition of ferroptosis rescues the PT cell plasticity after IRI

Genetic *Nrf2* deletion increased the number of 4-HNE and TUNEL^{+} cells in IRI kidneys, suggesting that NRF2 controls PT cell fate by mitigating ferroptotic stress and inhibiting ferroptosis. To directly evaluate the contribution of NRF2 in regulating ferroptotic stress, we administered liproxstatin-1 (Lip-1), an *in vivo* scavenger of toxic lipid peroxides that inhibits ferroptosis (Friedmann Angeli et al., 2014; Ide and Souma, 2022), to our *Nrf2* cKO mice that underwent renal IRI (cKO, Lip-1), (Figure 6A). The same volume of vehicle solution (1% dimethyl sulfoxide in phosphate-buffered saline) was administered to cKO mice that underwent the same ischemic stress and tamoxifen injections (cKO, vehicle).

Vehicle-treated cKO kidneys show accumulation of SOX9^{+} VCAM1^{+} inflammatory PT cells on day 21 after IRI, whereas daily Lip-1 treatment significantly reduced the number of these cells (Figures 6B and 6C). To follow the fate of SOX9^{+} cells after *Nrf2* deletion, we then introduced the *Rosa26*^{tdTomato} lineage reporter in this mouse line (*Sox9*^{CreERT2}; *Nrf2*$^{flox/flox}$; *Rosa26*^{tdTomato}) (Ide et al., 2021). We observed a significant reduction of VCAM1 expression, a molecular marker for failed repair state (Kirita et al., 2020), in *Nrf2*-deleted *Sox9*-lineage cells in Lip-1-treated IRI kidneys compared with the vehicle-treated IRI kidneys (Figures 6D and 6E). This result indicates that Lip-1 improved the plasticity of *Sox9*-lineage cells and facilitated their re-differentiation to a normal quiescent state (Figure 6F). Moreover, we observed a marked reduction of 4-HNE and TUNEL^{+} cells in IRI kidneys from Lip-1-treated *Nrf2* cKO mice compared with vehicle-treated cKO mice (Figures 6G–6J). Collectively, these data substantiate our previously proposed model (Ide et al., 2021) that ferroptotic stress drives the accumulation of inflammatory PT cells by preventing their re-differentiation and identify NRF2 as the key *in vivo* regulator of PT cell fate and plasticity by inhibiting ferroptotic stress (Figure 6K).

Pharmacological activation of NRF2 protects kidneys from ferroptosis

Next, we tested our hypothesis that induction of NRF2 renders male PT cells resistant to ferroptosis *in vivo* like female PT cells. We administered a pharmacological activator of NRF2 (CDDO-Im, 16 mg/kg body weight) by oral gavage to the *Gpx4* cKO mice and their *Gpx4*-intact littermates (Figure 7A). In addition, vehicle solution was administered to each genotype of mice as controls. CDDO-Im improved kidney function in *Gpx4* cKO mice (Figure 7B) and potently induced the genes associated with female resilience to ferroptosis in *Gpx4*-deleted male kidneys, as hypothesized (Figure S10B). Vehicle-treated *Gpx4* cKO kidneys showed an increase in KIM1 expression and the accumulation of $SOX9^{+}VCAM1^{+}$ inflammatory PT cells after *Gpx4* deletion, whereas CDDO-Im treatment significantly mitigated these pathological changes (Figures 7C and 7D; Figures S10C and S10D). Moreover, we observed a significant reduction of $TUNEL^{+}$ cells by CDDO-Im in *Gpx4* cKO mice compared with vehicle-treated cKO mice (Figures 7E and 7F). The improvement in tubular injury and cell death in CDDO-Im-treated *Gpx4* cKO mice was associated with reduced 4-HNE, macrophage accumulation, and collagen 1 deposition (Figures S10E–S10H).

We then tested whether CDDO-Im-mediated protection is cell autonomous and conserved across species using a cell-based assay. We subjected human and pig PT cell lines (HK2 and LLC-PK1, respectively) with a ferroptosis inducer, erastin (Dixon et al., 2012). CDDO-Im effectively prevented erastin-induced ferroptosis in both human and pig PT cells (Figure 7G) but failed to rescue *Nrf2*-deficient MEFs from ferroptotic death (Figure 7H), supporting our contention that NRF2 activation in PT cells mitigates ferroptosis of these cells across species. Collectively, our results strongly suggest that NRF2 is a central regulator of ferroptosis sensitivity and a critical determinant of PT cell fate and plasticity *in vivo* (Figures 6K and 7I).

DISCUSSION

Identifying the mechanisms that regulate ferroptosis is critical for designing therapeutic interventions to a wide range of human pathologies, such as cardiovascular diseases, neurodegeneration, chemotherapy-resistant cancers, ischemia reperfusion, and acute and chronic kidney diseases (Jiang et al., 2021; Zou and Schreiber, 2020). Multiple high-throughput cell-based screening assays have been applied to advance the field (Jiang et al., 2021; Zou and Schreiber, 2020). However, the molecular mechanisms governing differential ferroptosis sensitivity *in vivo* are poorly understood. In this study, we uncovered that ferroptosis sensitivity of PT cells is markedly different between sexes. We show that PT cells in female kidneys are resistant to ferroptosis, whereas male PT cells are vulnerable. Mechanistically, our single-cell transcriptomic analyses find distinct regulatory nodes that likely determine PT cell state and sensitivity to ferroptosis and identify NRF2 as a key molecule that underpins ferroptosis resilience in female cells. Our study also establishes a critical role for NRF2 in regulating cell fate and plasticity in adaptive reprogramming processes of kidney injury and repair by inhibiting ferroptotic stress.

Based on our surprising finding that female PT cells are markedly resistant to ferroptosis *in vivo*, we reasoned that by defining and comparing cell states of both sexes after genetic

perturbation, we could identify molecular regulators of differential ferroptosis sensitivity at single-cell resolution *in vivo*. Through unbiased computational inference, we found a distinct pattern of regulatory nodes in normal and *Gpx4*-deleted PT cells from both sexes. Some regulatory nodes are already highly enriched in PT cells at baseline in females, and others emerge in the *Gpx4*-deficient state, suggesting that female ferroptosis resilience is both constitutive and adaptive. Moreover, we found that female resistance to ferroptosis is significantly, but partly, conferred by the female sex hormonal environment, supporting the idea that the regulation of ferroptosis sensitivity involves multiple interactions between cells and their environment. Our data also provide mechanistic insight into the clinical observation that the female hormonal environment protects, and the male hormonal environment aggravates, acute and chronic kidney injuries (Aufhauser et al., 2016; Bairey Merz et al., 2019; Harris and Zhang, 2020). In light of the fact that female PT cells undergo cyclic stress during the estrous cycle in humans (Seppi et al., 2016), we surmise that female resilience to ferroptosis is part of a natural system that guards against the cyclic changes of microenvironment and physiological increase of metabolic demand that strains renal tubular cells during pregnancy, as in the other systems (Nakada et al., 2014).

Our scRNA-seq analyses identified NRF2, a cap'n'collar (CNC) transcription factor and the master regulator of antioxidative stress responses (Yamamoto et al., 2018), as the top candidate for female ferroptosis resilience. Several lines of evidence implicate NRF2 as a critical regulator of acute and chronic kidney diseases. Genome-wide association studies identify single-nucleotide polymorphisms near the *NRF2* locus with kidney function (Morris et al., 2019), and NRF2 serves as a signaling hub for human CKD progression (Martini et al., 2014). Preclinical studies support the protective role of NRF2 in AKI (Liu et al., 2014; Nezu et al., 2017), and pharmacological activators of NRF2 are under phase 2/3 clinical trials for multiple forms of kidney diseases (Ito et al., 2020; Yamamoto et al., 2018). However, given the increasing attention on NRF2 inhibition as a therapeutic strategy for therapy-resistant cancers and concern about a cardiovascular adverse event tied to use of an NRF2 inducer in a clinical trial on advanced diabetic kidney disease (Ito et al., 2020; Yamamoto et al., 2018), we need to deepen our understanding of the NRF2 pathway and identify downstream molecular and cellular regulators that can be targeted in human populations at risk.

Through pharmacological gain-of-function, genetic loss-of-function, and genetic lineage-tracing studies, we found that NRF2 governs PT cell fate and plasticity by inhibiting ferroptosis. Thus, NRF2 controls cell fate and plasticity in terminally differentiated epithelial cells in their adaptive reprogramming during tissue injury and repair (Jessen et al., 2015; Tata et al., 2021), in addition to regulating stem cell renewal and differentiation (Dai et al., 2020). Our data also provide direct preclinical evidence that NRF2 is a therapeutic target to modulate ferroptosis sensitivity *in vivo*. Moreover, our finding that a low expression level of the *Gstm1* gene is associated with high occurrence of ferroptosis may explain the clinical observation that null mutation in *GSTM1* increases the risk of end-stage kidney disease in humans (Tin et al., 2017). Interestingly, higher consumption of NRF2-inducing diets was associated with better renal outcomes in this population, and *Gstm1*-null mice exhibit much higher lipid peroxidation in chronic kidney injury models (Gigliotti et al.,

2020). Therefore, we anticipate that the *GSTM1*-null population may benefit from NRF2 induction or ferroptosis inhibition when kidneys are damaged acutely.

In summary, our data establish that the NRF2 pathway is a potent inhibitor of ferroptosis *in vivo* in kidneys and substantiate our model in which NRF2 acts as a "molecular rheostat" modulating ferroptosis sensitivity, thus governing cell fate and plasticity (Figure 7I). More broadly, our results pinpoint the significant possibility that endogenous female resilience factors can be therapeutically harnessed to inhibit ferroptosis in both sexes during AKI in order to prevent transition to CKD.

Limitations of the study

Using tamoxifen-inducible *Gpx4* KO mouse lines, prior studies showed the critical role of GPX4 in maintaining tubular epithelial health (Friedmann Angeli et al., 2014; Van Coillie et al., 2022). They reported early lethality due to severe AKI. To avoid the potential bias of tamoxifen, a selective estrogen receptor modulator, in sex hormonal effects on kidney injury and repair processes, we selectively used a doxycycline-inducible, tubule-specific *Gpx4* KO mouse line. Potentially due to the differences in genetic targeting strategies, our model showed a milder AKI phenotype compared with the previous reports and avoided the reported early lethality. Additional studies are needed to determine the precise molecular mechanisms as to how our *Gpx4* cKO mice circumvented the lethality and whether sex differences in ferroptosis are observed in other models and tissues.

STAR★METHODS

RESOURCE AVAILABILITY

Lead contact—Further information and requests for resources and reagents should be directed to and will be fulfilled by the lead contact, Tomokazu Souma (tomokazu.souma@duke.edu).

Materials availability—This study did not generate new unique materials. All mouse lines used in this manuscript are available from the Jackson Laboratory.

Data and code availability—Single-cell RNA-seq data that support the findings of this study have been deposited at Gene Expression Omnibus (GEO, GEO accession: GSE197528) and are publicly available as of the date of publication. All other data reported in this paper will be shared by the lead contact upon request.

This paper does not report original code.

Any additional information required to reanalyze the data reported in this paper is available from the lead contact upon request.

EXPERIMENTAL MODEL AND SUBJECT DETAILS

Animal studies—All animal experiments were approved by the Institutional Animal Care and Use Committee at Duke University (A051–18-02 and A014–21-01) and conform to the NIH Guide for the Care and Use of Laboratory Animals. Animal husbandry

and veterinary care were provided by Duke University's Division of Laboratory Animal Resources (DLAR). Male and female mice aged between 4 and 16 weeks were used for the studies. The following mouse lines were used for our study: *Pax8rtTA* (Jackson lab, stock #007176), *tetO-Cre* (Jackson lab, stock #006234), *Gpx4*^{flox} (Jackson lab, stock# 027964), *Nrf2*^{flox} (Jackson lab, stock# 025433), *Rosa26*^{tdTomato} (Jackson lab, stock #007914), *Sox9*$^{IRES\text{-}CreERT2}$, and C57BL/6J (Jackson lab, stock# 000664) (Kong et al., 2011; Madisen et al., 2010; Perl et al., 2002; Soeda et al., 2010; Traykova-Brauch et al., 2008; Yoo et al., 2012). Mice were backcrossed into a C57BL/6J background at least 4 times and maintained in our specific-pathogen-free facility. Mice were genotyped using the primers listed in Table S1. Timed genetic deletion of target genes was achieved as follows. We deleted *Gpx4* in renal tubular epithelial cells by using a *Pax8rtTA*; *tetO-Cre* system (Traykova-Brauch et al., 2008) with doxycycline treatment in drinking water (0.2% (wt/vol) doxycycline and 5% (wt/vol) sucrose) for 7 days. For the long-term observational study (day 28), these mice were further fed with a doxycycline-containing diet (625 mg/kg, TD.08541, Envigo, Indianapolis, IN). Deletion of *Nrf2* in *Sox9*-lineage cells was achieved using a *Sox9*$^{IRES\text{-}CreERT2}$ system (Ide et al., 2021; Soeda et al., 2010) with 3 doses of intraperitoneal injections of tamoxifen (100 mg/kg body weight, Sigma, St. Louis MO) on alternate days. The first dose of tamoxifen was administered immediately before the surgical intervention. Control mice were subjected to the same drug treatment regimen. To avoid confounding effects of age and strain background, littermate controls were used for all phenotypic analyses of genetically modified mouse lines, and the data were combined to obtain the experimental sample sizes. Serum creatinine levels were measured at Bioanalytical Core of O'Brien Center for Acute Kidney Injury Research, University of Alabama at Birmingham using LC-mass spectrometry.

Cell culture studies—Human and pig male proximal tubular cell lines (HK2, ATCC, CRL-2190; LLC-PK1, ATCC, CL-101) were obtained from the Cell Culture Facility (CCF) at Duke University. Wild-type and *Nrf2* knockout male mouse embryonic fibroblasts (MEFs) were a generous gift from Drs. Wakabayashi, Yagishita, and Kensler (Wakabayashi et al., 2010). Cells were seeded on 96-well tissue culture assay plates at 2,500 cells/well with 3 biological replicates per condition, and they were cultured with standard methods in a humidified incubator at 37°C with 5% CO_2. HK2 and LLC-PK1 cells were cultured in DMEM high glucose (Corning) supplemented with 10% fetal bovine serum (Corning, 35–010-CV) and 1% penicillin/streptomycin (Sigma). MEFs were cultured in IMDM (Thermo, 76,050) supplemented with 10% fetal bovine serum and 1% primocin (Invivogen, ANT-PM-1) (Wakabayashietal.,2010). Cells were tested to be mycoplasma free by Duke CCF. The cell lines have not been authenticated in our lab.

METHOD DETAILS

Surgical models—Mice were anesthetized with isoflurane and provided preemptive analgesics (buprenorphine SR). The body temperature of mice was monitored and maintained on a heat-controlled surgical pad. Adult male mice aged between 8 and 16 weeks were used for unilateral IRI with mild ischemic time (20 min) using an atraumatic vascular clip (Roboz, RS-5435, Gaithersburg, MD). We induced ischemia by clamping the left renal pedicle through dorsal incision (Ide et al., 2021). Contralateral kidneys (CLK)

and vehicle-injected kidneys were used as controls as described in the individual figure legends and experimental schemes. Juvenile female mice aged 4–5 weeks old were subjected to ovariectomy (OVX). Ovaries were exposed and located through dorsal single midline incision. The ovaries were then isolated, ligated, and removed. Sham-treated animals underwent the same surgical procedure except the ovaries were left intact. All animals were allowed to recover for 4 weeks before initiating doxycycline feeding to genetically delete the *Gpx4* gene. Adult male mice aged 7–9 weeks old were subjected to orchiectomy (ORX). Testes were exposed and located through single ventral incision on scrotal sac. Testes were then isolated, ligated, and removed. Sham-treated animals underwent the same surgical procedure except testes were left intact. All animals were allowed to recover for 3 weeks before harvesting kidneys. The operators were blinded to mouse genotypes when inducing surgical injury models.

Pharmacological ferroptosis inhibition—Pharmacological inhibition of ferroptosis in mice was performed using liproxstatin-1 (Lip-1; (Friedmann Angeli et al., 2014; Ide et al., 2021). Mice were randomly assigned to vehicle (1% dimethyl sulfoxide in phosphate-buffered saline) and Lip-1 (10 mg/kg, Selleckchem, S7699) groups. Mice were administered either vehicle or Lip-1 daily by intraperitoneal injections starting from 1 h before renal ischemia. All the mice were subjected to the same ischemic stress (20-min ischemic time) and tamoxifen treatment to avoid potential confounding. The mice were euthanized, and kidneys were harvested on day 21 after IRI.

Pharmacological activation of NRF2—CDDO-Im (Tocris Bioscience, #47–371-0) was dissolved in vehicle (10% dimethyl sulfoxide, 10% Kolliphor-EL [Sigma, C5135] in PBS) and administered at 30 μmol/kg body weight orally to mice on alternate days (Nezu et al., 2017). Vehicle was administered to control group. Mice were euthanized at indicated time points in the scheme and figure legend.

scRNAseq—To prepare single-cell suspension of whole kidneys, the kidneys were dissociated with liberase TM (0.3 mg/mL, Roche, Basel, Switzerland, #291963), hyaluronidase (10 μg/mL, Sigma, H4272), DNaseI (20 μg/mL) at 37°C for 20 min, followed by incubation with 0.25% trypsin EDTA at 37°C for 10 min. Trypsin was inactivated using 10% fetal bovine serum in PBS. Cells were then resuspended in PBS supplemented with 0.01% BSA. Our protocol yielded high cell viability (>90%) and very few doublets (Ide et al., 2021). After filtration through a 40 μm strainer, cells were processed at the Viral Genetic Analysis Core Facility at Duke Human Vaccine Institute. The samples were targeted to 10,000 cell recovery and processed using 10x Chromium Single Cell 3' Reagent kit v3.1 (10x Genomics, Pleasanton, CA). cDNA libraries were sequenced using HiSeq X Ten with 150-bp paired-end sequencing. Each condition contains the cells from two mice to minimize potential biological and technical variability.

Data preprocessing, unsupervised clustering, and cell type annotation—Analysis of the scRNAseq of mouse kidneys was performed by processing FASTQ files using 10x Genomics Cell Ranger (ver. 6.0.1), and reads were mapped on the mm10 mouse genome reference. Unique molecular identifier (UMI) counts were then further analyzed

using an R package Seurat v.4.06 for quality control, dimensionality reduction, and cell clustering (Hao et al., 2021). The scRNAseq matrices were filtered by custom cutoff (genes expressed in >1 cells, cells expressing more than 300 and less than 7,500 detected genes, and cells with %mitochondrial genes<0.7 were included) to remove potential empty droplets and doublets. Relationships between the number of UMI/cell and genes/cell were comparable across the condition (Figure S3A). DoubletFinder (ver. 2.03) and SoupX (ver. 1.5.2) were used to remove predicted doublets and ambient RNA contamination (McGinnis et al., 2019; Young and Behjati, 2020). After these quality control steps, the filtered libraries were normalized using SCTransform (Hafemeister and Satija, 2019). To remove an additional confounding source of variation, the mitochondrial mapping percentage was regressed out. UMI count matrices from each condition were integrated using Seurat's integration and label transfer method, which corrects potential batch effects (Chazarra-Gil et al., 2021; Hao et al., 2021). The integrated dataset was used for all the downstream analyses. The number of principal components (PC) for downstream analyses were determined using elbow plot to identify knee point, and we included the first 25 PCs for the downstream analyses. A graph-based clustering approach in Seurat was used to cluster the cells in our integrated dataset, and the resolution was set at 2.0. Cluster-defining markers for each cluster were obtained using the Seurat's FindAllMarkers command (genes at least expressed in 20% of cells within the cluster, log fold change> 0.25) with the Wilcoxon Rank-Sum test. Based on the marker genes and manual curation of the gene expression pattern of canonical marker genes in UMAP plots, we assigned a cell identity to each cluster. We manually combined clusters of proximal tubular cells from different segments (S1, S2, and S3) into 1 cluster (PT) to generate a more coarse-grained cell-type annotation and data visualization.

Differential gene expression analyses—To predict signaling pathways governing cell state, we performed Enrichr analyses using differentially expressed genes obtained by FindMarkers command in Seurat with Wilcoxon rank-sum test (Kuleshov et al., 2016). Log_2 fold changes and p-values of each gene extracted were shown in a volcano plot using an R package EnhancedVolcano v1.10.0 (Figure S5A and supplementary data files). The top 100 genes in inflammatory PT cells in the ischemia-reperfusion-injured kidneys were obtained from GSE161201 and used as a gene list characterizing inflammatory PT cells (Supplementary data file 1). The mean values of the scaled scores for this gene list were calculated and visualized in the UMAP plot.

Pseudotime trajectory analyses—To infer the dynamic cellular process after *Gpx4* deletion, we performed single-cell trajectory analyses on the clusters of interest (PT and DA-PT) in our integrated Seurat object. We used Monocle 3 (version 1.0.0) with default parameters to identify a pseudotime trajectory (Cao et al., 2019). We used the UMAP space area occupied by the cells with high *Slc34a1*, a gene that is highly expressed in differentiated PT cells as the starting state.

Gene regulatory network analysis—To predict candidate transcription factors governing each cell state, we used SCENIC (ver.1.2.4), which infers the gene regulatory network based on co-expression of transcription factors and their target genes with cis-regulatory sequence information. Based on the workflow provided by Aerts lab (Aibar et

al., 2017), we included the genes with at least 6 UMI counts and detected at least in 10% of PT cells for downstream analyses. Network regulatory activity was analyzed in each PT cell from our integrated Seurat object with all conditions. Regulon activity of each cell was then scored using AUCell and projected onto UMAP, and the average regulon activities were clustered based on experimental condition and shown as heatmap.

Tissue collection and histology—Kidneys were prepared as follows. For cryosections (7 μm), the tissues were fixed with 4% paraformaldehyde in PBS at 4°C for 4 h and then processed through a sucrose gradient. Kidneys were embedded in OCT compound for sectioning. For paraffin sections (5 μm), the tissues were fixed with 10% neutral buffered formalin overnight at 4°C and processed at Substrate Services Core & Research Support at Duke. Sections were blocked (animal-free blocker [Vector, SP-5030], with 0.5% Triton x-100) for 30 min and incubated with the primary antibodies overnight at 4°C. Primary antibodies used were as follows: KIM1 (R&D Systems, Minneapolis, MN, AF1817, 1:400), NGAL (Abcam, ab70287, 1:400), COL1A1 (CST, E8F4L, 1:200), F4/80 (Bio-rad, Hercules, CA, MCA497G, 1:200), SOX9 (Abcam, Cambridge, UK, ab196450 or ab185966, 1:200), VCAM1 (CST, 39036S or 33901S, 1:200), LTL (Vector, Burlingame, CA, FL-1321, 1:200), 4-HNE (Abcam, ab46545, 1:200), cleaved caspase 3 (CST, 9661S, 1:400), ACSL4 (Abcam, Ab155282, 1:200), and GPX4 (Abcam, ab125066, 1:200). Alexa Fluor-labeled secondary antibodies were used appropriately for immunofluorescence. ImmPRESS HRP reagent kit was used for immunohistochemistry (Vector, MP-7401). Heat-induced antigen retrieval was performed using pH 6.0 sodium citrate solution (eBioscience). Experiments for RNAScope *in situ* hybridization was performed as recommended by the manufacturer using Multiplex Fluorescent Reagent Kit v.2 (Cat. #323100, Advanced Cell Diagnostics, ACD, Newark, CA) and RNA Protein Co Detection kit (Cat. #323180). The following probes were used: Mm-*Gstm1* (ACD, 503,461), Mm-*Gsta4* (ACD, 1,132,411), and Mm-*Mgst1* (ACD, 861,961). TUNEL staining was performed following the manufacturer's instruction (Abcam, ab206386). To ensure the TUNEL signal's specificity, we used sections treated with DNase I as a positive control and a section treated without terminal deoxynucleotidyl transferase as a negative control, as recommended by the manufacturer. Sections stained for TUNEL were counterstained with methyl green. To evaluate apoptosis, we used spleens from the mice subjected to a single dose of 5 mg/kg lipopolysaccharide (LPS, E. Coli serotype O111:B4; Sigma, L2630) intraperitoneally and harvested 24 h after injection as a positive control. Periodic acid Schiff (PAS) staining was performed following manufacturer's protocol (Sigma, 395B). Images were captured using Axio imager and 780 confocal microscopes (Zeiss, Oberkochen, Germany). More than three randomly selected areas from at least three kidneys were imaged and quantified using ImageJ (Ide et al., 2021). Quantifications were performed by two independent investigators to ensure reproducibility. Stitched large areas were used for quantification to alleviate the selection bias in the acquisition of images. All representative images were from more than 3 kidneys tested.

RNA extraction and real-time quantitative PCR—Total RNA was extracted from kidneys using the TRIzol reagent (Invitrogen, 15,596,026). 3 μg of total RNA was reverse transcribed with Maxima H minus cDNA synthesis master mix (Invitrogen, M1662), and equivalent amounts of diluted cDNA from each sample were analyzed with real-time PCR

with the primers listed in Table S2 using the Powerup SYBR Green reagent (Invitrogen, A25776) on a QuantStudio 3 real-time PCR systems (Thermo). 18S rRNA expression was used to normalize samples using the ΔΔCT-method.

Cell culture—To induce ferroptosis, cells were incubated with erastin (Tocris, 5449) for 48 h, then cellular viability was evaluated with PrestoBlue viability reagent (Invitrogen, A13262) on a microplate reader (BMG labtech, Fluostar Optima). CDDO-Im (100 nM for LLC-PK1 and 10 nM for HK2 and MEF cells) or vehicle (dimethyl sulfoxide) were pretreated for 24 h to evaluate the contribution of NRF2 in ferroptosis. Cellular viability assays were repeated at least for 3 times, and representative experimental results are shown (all experiments showed the same trend). Relative viability was normalized to the respective erastin-free conditions. Sigmoidal nonlinear regression models were used to compute the regression fitting curves using GraphPad Prism.

QUANTIFICATION AND STATISTICAL ANALYSIS

All statistical analyses were performed using GraphPad Prism software. Statistical methods relevant to each figure are outlined in the figure legend. To determine experimental sample sizes to observe significant differences reproducibly, data from our previous studies were used to estimate the required animal numbers. The number of biological replicates is represented by n in each figure legend. Experiments were performed on at least three biological replicates. Each graphed point corresponds to a single biological replicate. Animals were allocated randomly into the experimental groups and analyses, while ensuring inclusion criteria based on sex, age, and genotypes. All tested animals were included in data analyses, and outliers were not excluded. In animal experiments, two-tailed unpaired Student's t-test was used for two groups, and one-way analysis of variance (ANOVA) followed by Sidak multiple comparison test was used for more than two groups. For cellular viability assays, two-way ANOVA followed by Sidak multiple comparison test was used. All results from *in vivo* experiments are represented as means ± SEM and results from cell-based assays are shown as means ± SD. A p value less than 0.05 was considered statistically significant.

Supplementary Material

Refer to Web version on PubMed Central for supplementary material.

ACKNOWLEDGMENTS

We thank Drs. Brigid Hogan and Myles Wolf for critical advice and helpful suggestions on the manuscript. We also thank Drs. Helene F. Kirshner and Jianhong Ou (Duke University) for bioinformatical support, and Suzanne Wardell (Duke University) and Iordan Batchvarov (Duke University) for their insightful and technical advice. This study was supported by grants from the National Institute of Diabetes and Digestive and Kidney Diseases (R01 DK123097); Duke DST spark seed grant; a pilot award from the Northwestern University George M. O'Brien Kidney Research Core Center (P30 DK114857); the American Society of Nephrology Carl W. Gottschalk Career Development Grant; and Duke Nephrology Start-up Fund to T.S. S.I., K.I., and K.A. are supported in part by fellowship grants from the American Heart Association, the Astellas Foundation for Research on Metabolic Disorders, and the Uehara Memorial Foundation, respectively. Imaging was performed at the Duke Light Microscopy Core Facility supported by the shared instrumentation grant (1S10RR027528-01).

INCLUSION AND DIVERSITY

We support inclusive, diverse, and equitable conduct of research.

REFERENCES

Aibar S, Gonzá lez-Blas CB, Moerman T, Huynh-Thu VA, Imrichova H, Hulselmans G, Rambow F, Marine JC, Geurts P, Aerts J, et al. (2017). SCENIC: single-cell regulatory network inference and clustering. Nat. Methods 14, 1083–1086. 10.1038/nmeth.4463. [PubMed: 28991892]

Aufhauser DD Jr., Wang Z, Murken DR, Bhatti TR, Wang Y, Ge G, Redfield RR 3rd, Abt PL, Wang L, Svoronos N, et al. (2016). Improved renal ischemia tolerance in females influences kidney transplantation outcomes. J. Clin. Invest 126, 1968–1977. 10.1172/JCI84712. [PubMed: 27088798]

Bagshaw SM, Laupland KB, Doig CJ, Mortis G, Fick GH, Mucenski M, Godinez-Luna T, Svenson LW, and Rosenal T. (2005). Prognosis for long-term survival and renal recovery in critically ill patients with severe acute renal failure: a population-based study. Crit. Care 9, R700–R709. 10.1186/cc3879. [PubMed: 16280066]

Bairey Merz CN, Dember LM, Ingelfinger JR, Vinson A, Neugarten J, Sandberg KL, Sullivan JC, Maric-Bilkan C, Rankin TL, Kimmel PL, et al. (2019). Sex and the kidneys: current understanding and research opportunities. Nat. Rev. Nephrol 15, 776–783. 10.1038/s41581-019-0208-6. [PubMed: 31586165]

Bellanti F, Matteo M, Rollo T, De Rosario F, Greco P, Vendemiale G, and Serviddio G. (2013). Sex hormones modulate circulating antioxidant enzymes: impact of estrogen therapy. Redox Biol. 1, 340–346. 10.1016/j.redox.2013.05.003. [PubMed: 24024169]

Balzer MS, Doke T, Yang YW, Aldridge DL, Hu H, Mai H, Mukhi D, Ma Z, Shrestha R, Palmer MB, et al. (2022). Single-cell analysis highlights differences in druggable pathways underlying adaptive or fibrotic kidney regeneration. Nat. Commun 13, 4018. 10.1038/s41467-022-31772-9. [PubMed: 35821371]

Bowe B, Xie Y, Xu E, and Al-Aly Z. (2021). Kidney outcomes in long COVID. J. Am. Soc. Nephrol 32, 2851–2862. 10.1681/ASN.2021060734. [PubMed: 34470828]

Cao J, Spielmann M, Qiu X, Huang X, Ibrahim DM, Hill AJ, Zhang F, Mundlos S, Christiansen L, Steemers FJ, et al. (2019). The single-cell transcriptional landscape of mammalian organogenesis. Nature 566, 496–502. 10.1038/s41586-019-0969-x. [PubMed: 30787437]

Chawla LS, Eggers PW, Star RA, and Kimmel PL (2014). Acute kidney injury and chronic kidney disease as interconnected syndromes. N. Engl. J. Med 371, 58–66. 10.1056/NEJMra1214243. [PubMed: 24988558]

Chazarra-Gil R, van Dongen S, Kiselev VY, and Hemberg M. (2021). Flexible comparison of batch correction methods for single-cell RNA-seq using BatchBench. Nucleic Acids Res. 49, e42. 10.1093/nar/gkab004. [PubMed: 33524142]

Dai X, Yan X, Wintergerst KA, Cai L, Keller BB, and Tan Y. (2020). Nrf2: redox and metabolic regulator of stem cell state and function. Trends Mol. Med 26, 185–200. 10.1016/j.molmed.2019.09.007. [PubMed: 31679988]

Dixon SJ, Lemberg KM, Lamprecht MR, Skouta R, Zaitsev EM, Gleason CE, Patel DN, Bauer AJ, Cantley AM, Yang WS, et al. (2012). Ferroptosis: an iron-dependent form of nonapoptotic cell death. Cell 149, 1060–1072. 10.1016/j.cell.2012.03.042. [PubMed: 22632970]

Eckenrode HE, Gutierrez OM, Osis G, Agarwal A, and Curtis LM (2022). Kidney disease prevalence in transgender individuals. Clin. J. Am. Soc. Nephrol 17, 280–282. 10.2215/CJN.04660421. [PubMed: 34872973]

Ferenbach DA, and Bonventre JV (2015). Mechanisms of maladaptive repair after AKI leading to accelerated kidney ageing and CKD. Nat. Rev. Nephrol 11, 264–276. 10.1038/nrneph.2015.3. [PubMed: 25643664]

Fisher M, Neugarten J, Bellin E, Yunes M, Stahl L, Johns TS, Abramowitz MK, Levy R, Kumar N, Mokrzycki MH, et al. (2020). AKI in hospitalized patients with and without COVID-19: a comparison study. J. Am. Soc. Nephrol 31, 2145–2157. 10.1681/ASN.2020040509. [PubMed: 32669322]

Friedmann Angeli JP, Schneider M, Proneth B, Tyurina YY, Tyurin VA, Hammond VJ, Herbach N, Aichler M, Walch A, Eggenhofer E, et al. (2014). Inactivation of the ferroptosis regulator Gpx4 triggers acute renal failure in mice. Nat. Cell Biol 16, 1180–1191. 10.1038/ncb3064. [PubMed: 25402683]

Gerhardt LMS, Liu J, Koppitch K, Cippà PE, and McMahon AP (2021). Single-nuclear transcriptomics reveals diversity of proximal tubule cell states in a dynamic response to acute kidney injury. Proc. Natl. Acad. Sci. USA 118, e2026684118. 10.1073/pnas.2026684118.

Gigliotti JC, Tin A, Pourafshar S, Cechova S, Wang YT, Sung SSJ, Bodonyi-Kovacs G, Cross JV, Yang G, Nguyen N, et al. (2020). GSTM1 deletion Exaggerates kidney injury in experimental mouse models and confers the protective effect of cruciferous Vegetables in mice and humans. J. Am. Soc. Nephrol 31, 102–116. 10.1681/ASN.2019050449. [PubMed: 31727850]

Goldstein SL, Jaber BL, Faubel S, and Chawla LS; Acute Kidney Injury Advisory Group of American Society of Nephrology (2013). AKI transition of care: a potential opportunity to detect and prevent CKD. Clin. J. Am. Soc. Nephrol 8, 476–483. 10.2215/CJN.12101112.

Grasl-Kraupp B, Ruttkay-Nedecky B, Koudelka H, Bukowska K, Bursch W, and Schulte-Hermann R. (1995). In situ detection of fragmented DNA (TUNEL assay) fails to discriminate among apoptosis, necrosis, and autolytic cell death: a cautionary note. Hepatology 21, 1465–1468. 10.1002/hep.1840210534. [PubMed: 7737654]

Guan Y, Liang X, Ma Z, Hu H, Liu H, Miao Z, Linkermann A, Hellwege JN, Voight BF, and Susztak K. (2021). A single genetic locus controls both expression of DPEP1/CHMP1A and kidney disease development via ferroptosis. Nat. Commun 12, 5078. 10.1038/s41467-021-25377-x. [PubMed: 34426578]

Hafemeister C, and Satija R. (2019). Normalization and variance stabilization of single-cell RNA-seq data using regularized negative binomial regression. Genome Biol. 20, 296. 10.1186/s13059-019-1874-1. [PubMed: 31870423]

Hao Y, Hao S, Andersen-Nissen E, Mauck WM 3rd, Zheng S, Butler A, Lee MJ, Wilk AJ, Darby C, Zager M, et al. (2021). Integrated analysis of multimodal single-cell data. Cell 184, 3573–3587.e29, e3529. 10.1016/j.cell.2021.04.048.

Harris RC, and Zhang MZ (2020). The role of gender disparities in kidney injury. Ann. Transl. Med 8, 514. 10.21037/atm.2020.01.23. [PubMed: 32395558]

Hayes JD, Flanagan JU, and Jowsey IR (2005). Glutathione transferases. Annu. Rev. Pharmacol. Toxicol 45, 51–88. 10.1146/annurev.pharmtox.45.120403.095857. [PubMed: 15822171]

Hsu RK, McCulloch CE, Dudley RA, Lo LJ, and Hsu CY (2013). Temporal changes in incidence of dialysis-requiring AKI. J. Am. Soc. Nephrol 24, 37–42. 10.1681/ASN.2012080800. [PubMed: 23222124]

Ichimura T, Asseldonk EJPV, Humphreys BD, Gunaratnam L, Duffield JS, and Bonventre JV (2008). Kidney injury molecule-1 is a phosphatidylserine receptor that confers a phagocytic phenotype on epithelial cells. J. Clin. Invest 118, 1657–1668. 10.1172/JCI34487. [PubMed: 18414680]

Ide S, Kobayashi Y, Ide K, Strausser SA, Abe K, Herbek S, O'Brien LL, Crowley SD, Barisoni L, Tata A, et al. (2021). Ferroptotic stress promotes the accumulation of pro-inflammatory proximal tubular cells in maladaptive renal repair. Elife 10, e68603. 10.7554/eLife.68603.

Ide K, and Souma T. (2022). In vivo assessment of ferroptosis and ferroptotic stress in mice. Curr. Protoc 2, e413. 10.1002/cpz1.413. [PubMed: 35384401]

Ingold I, Berndt C, Schmitt S, Doll S, Poschmann G, Buday K, Roveri A, Peng X, Porto Freitas F, Seibt T, et al. (2018). Selenium utilization by GPX4 is required to prevent hydroperoxide-induced ferroptosis. Cell 172, 409–422.e21, e421. 10.1016/j.cell.2017.11.048.

Ito M, Tanaka T, and Nangaku M. (2020). Nuclear factor erythroid 2-related factor 2 as a treatment target of kidney diseases. Curr. Opin. Nephrol. Hypertens 29, 128–135. 10.1097/MNH.0000000000000556. [PubMed: 31592832]

Jessen KR, Mirsky R, and Arthur-Farraj P. (2015). The role of cell plasticity in tissue repair: adaptive cellular reprogramming. Dev. Cell 34, 613–620. 10.1016/j.devcel.2015.09.005. [PubMed: 26418293]

Jiang X, Stockwell BR, and Conrad M. (2021). Ferroptosis: mechanisms, biology and role in disease. Nat. Rev. Mol. Cell Biol 22, 266–282. 10.1038/s41580-020-00324-8. [PubMed: 33495651]

Kang HM, Huang S, Reidy K, Han SH, Chinga F, and Susztak K. (2016). Sox9-Positive progenitor cells Play a key role in renal tubule epithelial regeneration in mice. Cell Rep. 14, 861–871. 10.1016/j.celrep.2015.12.071. [PubMed: 26776520]

Kirita Y, Wu H, Uchimura K, Wilson PC, and Humphreys BD (2020). Cell profiling of mouse acute kidney injury reveals conserved cellular responses to injury. Proc. Natl. Acad. Sci. USA 117, 15874–15883. 10.1073/pnas.2005477117.

Kong X, Thimmulappa R, Craciun F, Harvey C, Singh A, Kombairaju P, Reddy SP, Remick D, and Biswal S. (2011). Enhancing Nrf2 pathway by disruption of Keap1 in myeloid leukocytes protects against sepsis. Am. J. Respir. Crit. Care Med 184, 928–938. 10.1164/rccm.2011020271OC. [PubMed: 21799073]

Kuang F, Liu J, Xie Y, Tang D, and Kang R. (2021). MGST1 is a redox-sensitive repressor of ferroptosis in pancreatic cancer cells. Cell Chem. Biol 28, 765–775.e5, e765. 10.1016/j.chembiol.2021.01.006.

Kuleshov MV, Jones MR, Rouillard AD, Fernandez NF, Duan Q, Wang Z, Koplev S, Jenkins SL, Jagodnik KM, Lachmann A, et al. (2016). Enrichr: a comprehensive gene set enrichment analysis web server 2016 update. Nucleic Acids Res. 44, W90–W97. 10.1093/nar/gkw377. [PubMed: 27141961]

Kumar S, Liu J, Pang P, Krautzberger AM, Reginensi A, Akiyama H, Schedl A, Humphreys BD, and McMahon AP (2015). Sox9 activation highlights a cellular pathway of renal repair in the acutely injured mammalian kidney. Cell Rep. 12, 1325–1338. 10.1016/j.celrep.2015.07.034. [PubMed: 26279573]

Lewington AJP, Cerdá J, and Mehta RL (2013). Raising awareness of acute kidney injury: a global perspective of a silent killer. Kidney Int. 84, 457–467. 10.1038/ki.2013.153. [PubMed: 23636171]

Li P, Jiang M, Li K, Li H, Zhou Y, Xiao X, Xu Y, Krishfield S, Lipsky PE, Tsokos GC, and Zhang X. (2021). Glutathione peroxidase 4-regulated neutrophil ferroptosis induces systemic autoimmunity. Nat. Immunol 22, 1107–1117. 10.1038/s41590-021-00993-3. [PubMed: 34385713]

Liang A, Wang Y, Woodard LE, Wilson MH, Sharma R, Awasthi YC, Du J, Mitch WE, and Cheng J. (2012). Loss of glutathione S-transferase A4 accelerates obstruction-induced tubule damage and renal fibrosis. J. Pathol 228, 448–458. 10.1002/path.4067. [PubMed: 22711583]

Linkermann A, Skouta R, Himmerkus N, Mulay SR, Dewitz C, De Zen F, Prokai A, Zuchtriegel G, Krombach F, Welz PS, et al. (2014). Synchronized renal tubular cell death involves ferroptosis. Proc. Natl. Acad. Sci. USA 111, 16836–16841. 10.1073/pnas.1415518111.

Liu J, Cui JY, Lu YF, Corton JC, and Klaassen CD (2021). Sex-Age-and race/ethnicity-dependent variations in drug-processing and NRF2-regulated genes in human livers. Drug Metab. Dispos 49, 111–119. 10.1124/dmd.120.000181. [PubMed: 33162398]

Liu J, Kumar S, Dolzhenko E, Alvarado GF, Guo J, Lu C, Chen Y, Li M, Dessing MC, Parvez RK, et al. (2017). Molecular characterization of the transition from acute to chronic kidney injury following ischemia/reperfusion. JCI Insight 2, 94716. 10.1172/jci.insight.94716.

Liu M, Reddy NM, Higbee EM, Potteti HR, Noel S, Racusen L, Kensler TW, Sporn MB, Reddy SP, and Rabb H. (2014). The Nrf2 triterpenoid activator, CDDO-imidazolide, protects kidneys from ischemia-reperfusion injury in mice. Kidney Int. 85, 134–141. 10.1038/ki.2013.357. [PubMed: 24088953]

Lu YA, Liao CT, Raybould R, Talabani B, Grigorieva I, Szomolay B, Bowen T, Andrews R, Taylor PR, and Fraser D. (2021). Single-nucleus RNA sequencing identifies new Classes of proximal tubular epithelial cells in kidney fibrosis. J. Am. Soc. Nephrol 32, 2501–2516. 10.1681/ASN.2020081143. [PubMed: 34155061]

Madisen L, Zwingman TA, Sunkin SM, Oh SW, Zariwala HA, Gu H, Ng LL, Palmiter RD, Hawrylycz MJ, Jones AR, et al. (2010). A robust and high-throughput Cre reporting and characterization system for the whole mouse brain. Nat. Neurosci 13, 133–140. 10.1038/nn.2467. [PubMed: 20023653]

Maremonti F, Meyer C, and Linkermann A. (2022). Mechanisms and models of kidney tubular necrosis and Nephron loss. J. Am. Soc. Nephrol 33, 472–486. 10.1681/ASN.2021101293. [PubMed: 35022311]

Martini S, Nair V, Keller BJ, Eichinger F, Hawkins JJ, Randolph A, Böger CA, Gadegbeku CA, Fox CS, Cohen CD, et al. (2014). Integrative biology identifies shared transcriptional networks in CKD. J. Am. Soc. Nephrol 25, 2559–2572. 10.1681/ASN.2013080906. [PubMed: 24925724]

Mauvais-Jarvis F, Bairey Merz N, Barnes PJ, Brinton RD, Carrero JJ, DeMeo DL, De Vries GJ, Epperson CN, Govindan R, Klein SL, et al. (2020). Sex and gender: modifiers of health, disease, and medicine. Lancet 396, 565–582. 10.1016/S0140-6736(20)31561-0. [PubMed: 32828189]

McGinnis CS, Murrow LM, and Gartner ZJ (2019). DoubletFinder: doublet detection in single-cell RNA sequencing data using artificial nearest neighbors. Cell Syst. 8, 329–337.e4, e324. 10.1016/j.cels.2019.03.003.

Mishima E, Sato E, Ito J, Yamada KI, Suzuki C, Oikawa Y, Matsuhashi T, Kikuchi K, Toyohara T, Suzuki T, et al. (2020). Drugs repurposed as Anti-ferroptosis Agents suppress organ damage, including AKI, by functioning as lipid Peroxyl radical scavengers. J. Am. Soc. Nephrol 31, 280–296. 10.1681/ASN.2019060570. [PubMed: 31767624]

Morris AP, Le TH, Wu H, Akbarov A, van der Most PJ, Hemani G, Smith GD, Mahajan A, Gaulton KJ, Nadkarni GN, et al. (2019). Trans-ethnic kidney function association study reveals putative causal genes and effects on kidney-specific disease aetiologies. Nat. Commun 10, 29. 10.1038/s41467-018-07867-7. [PubMed: 30604766]

Müller T, Dewitz C, Schmitz J, Schröder AS, Bräsen JH, Stockwell BR, Murphy JM, Kunzendorf U, and Krautwald S. (2017). Necroptosis and ferroptosis are alternative cell death pathways that operate in acute kidney failure. Cell. Mol. Life Sci 74, 3631–3645. 10.1007/s00018-017-2547-4. [PubMed: 28551825]

Nadim MK, Forni LG, Mehta RL, Connor MJ Jr., Liu KD, Ostermann M, Rimmelé T, Zarbock A, Bell S, Bihorac A, et al. (2020). COVID-19-associated acute kidney injury: consensus report of the 25th Acute Disease Quality Initiative (ADQI) Workgroup. Nat. Rev. Nephrol 16, 747–764. 10.1038/s41581-020-00356-5. [PubMed: 33060844]

Nakada D, Oguro H, Levi BP, Ryan N, Kitano A, Saitoh Y, Takeichi M, Wendt GR, and Morrison SJ (2014). Oestrogen increases haematopoietic stem-cell self-renewal in females and during pregnancy. Nature 505, 555–558. 10.1038/nature12932. [PubMed: 24451543]

Neugarten J, and Golestaneh L. (2018). Female sex reduces the risk of hospital-associated acute kidney injury: a meta-analysis. BMC Nephrol. 19, 314. 10.1186/s12882-018-1122-z. [PubMed: 30409132]

Neugarten J, Golestaneh L, and Kolhe NV (2018). Sex differences in acute kidney injury requiring dialysis. BMC Nephrol. 19, 131. 10.1186/s12882-018-0937-y. [PubMed: 29884141]

Nezu M, Souma T, Yu L, Suzuki T, Saigusa D, Ito S, Suzuki N, and Yamamoto M. (2017). Transcription factor Nrf2 hyperactivation in early-phase renal ischemia-reperfusion injury prevents tubular damage progression. Kidney Int. 91, 387–401. 10.1016/j.kint.2016.08.023. [PubMed: 27789056]

Oppermann U. (2007). Carbonyl reductases: the complex relationships of mammalian carbonyl- and quinone-reducing enzymes and their role in physiology. Annu. Rev. Pharmacol. Toxicol 47, 293–322. 10.1146/annurev.pharmtox.47.120505.105316. [PubMed: 17009925]

Paragas N, Qiu A, Zhang Q, Samstein B, Deng SX, Schmidt-Ott KM, Viltard M, Yu W, Forster CS, Gong G, et al. (2011). The Ngal reporter mouse detects the response of the kidney to injury in real time. Nat. Med 17, 216–222. 10.1038/nm.2290. [PubMed: 21240264]

Perl AKT, Wert SE, Nagy A, Lobe CG, and Whitsett JA (2002). Early restriction of peripheral and proximal cell lineages during formation of the lung. Proc. Natl. Acad. Sci. USA 99, 10482–10487. 10.1073/pnas.152238499. [PubMed: 12145322]

Ransick A, Lindström NO, Liu J, Zhu Q, Guo JJ, Alvarado GF, Kim AD, Black HG, Kim J, and McMahon AP (2019). Single-cell profiling reveals sex, lineage, and regional diversity in the mouse kidney. Dev. Cell 51, 399–413.e7, e397. 10.1016/j.devcel.2019.10.005.

Rooney J, Oshida K, Vasani N, Vallanat B, Ryan N, Chorley BN, Wang X, Bell DA, Wu KC, Aleksunes LM, et al. (2018). Activation of Nrf2 in the liver is associated with stress resistance mediated by suppression of the growth hormone-regulated STAT5b transcription factor. PLoS One 13, e0200004. 10.1371/journal.pone.0200004.

Seppi T, Prajczer S, Dörler MM, Eiter O, Hekl D, Nevinny-Stickel M, Skvortsova I, Gstraunthaler G, Lukas P, and Lechner J. (2016). Sex differences in renal proximal tubular cell Homeostasis. J. Am. Soc. Nephrol 27, 3051–3062. 10.1681/ASN.2015080886. [PubMed: 27127188]

Soeda T, Deng JM, de Crombrugghe B, Behringer RR, Nakamura T, and Akiyama H. (2010). Sox9-expressing precursors are the cellular origin of the cruciate ligament of the knee joint and the limb tendons. Genesis 48, 635–644. 10.1002/dvg.20667. [PubMed: 20806356]

Sun X, Ou Z, Chen R, Niu X, Chen D, Kang R, and Tang D. (2016). Activation of the p62-Keap1-NRF2 pathway protects against ferroptosis in hepatocellular carcinoma cells. Hepatology 63, 173–184. 10.1002/hep.28251. [PubMed: 26403645]

Takahashi N, Cho P, Selfors LM, Kuiken HJ, Kaul R, Fujiwara T, Harris IS, Zhang T, Gygi SP, and Brugge JS (2020). 3D culture models with CRISPR Screens reveal hyperactive NRF2 as a prerequisite for Spheroid Formation via regulation of proliferation and ferroptosis. Mol. Cell 80, 828–844.e6, e826. 10.1016/j.molcel.2020.10.010.

Tata A, Chow RD, and Tata PR (2021). Epithelial cell plasticity: breaking boundaries and changing landscapes. EMBO Rep. 22, e51921. 10.15252/embr.202051921.

Tin A, Scharpf R, Estrella MM, Yu B, Grove ML, Chang PP, Matsushita K, Köttgen A, Arking DE, Boerwinkle E, et al. (2017). The loss of GSTM1 Associates with kidney failure and heart failure. J. Am. Soc. Nephrol 28, 3345–3352. 10.1681/ASN.2017030228. [PubMed: 28720685]

Traykova-Brauch M, Schö nig K, Greiner O, Miloud T, Jauch A, Bode M, Felsher DW, Glick AB, Kwiatkowski DJ, Bujard H, et al. (2008). An efficient and versatile system for acute and chronic modulation of renal tubular function in transgenic mice. Nat. Med 14, 979–984. 10.1038/nm.1865. [PubMed: 18724376]

Van Coillie S, Van San E, Goetschalckx I, Wiernicki B, Mukhopadhyay B, Tonnus W, Choi SM, Roelandt R, Dumitrascu C, Lamberts L, et al. (2022). Targeting ferroptosis protects against experimental (multi)organ dysfunction and death. Nat. Commun 13, 1046. 10.1038/s41467-022-28718-6. [PubMed: 35210435]

Wakabayashi N, Shin S, Slocum SL, Agoston ES, Wakabayashi J, Kwak MK, Misra V, Biswal S, Yamamoto M, and Kensler TW (2010). Regulation of notch1 signaling by nrf2: implications for tissue regeneration. Sci. Signal 3, ra52. 10.1126/scisignal.2000762.

Wenzel SE, Tyurina YY, Zhao J, St Croix CM, Dar HH, Mao G, Tyurin VA, Anthonymuthu TS, Kapralov AA, Amoscato AA, et al. (2017). PEBP1 Wardens ferroptosis by enabling Lipoxygenase generation of lipid death signals. Cell 171, 628–641.e26, e626. 10.1016/j.cell.2017.09.044.

Yamamoto M, Kensler TW, and Motohashi H. (2018). The KEAP1-NRF2 system: a thiol-based sensor-effector Apparatus for maintaining redox Homeostasis. Physiol. Rev 98, 1169–1203. 10.1152/physrev.00023.2017. [PubMed: 29717933]

Yang WS, SriRamaratnam R, Welsch ME, Shimada K, Skouta R, Viswanathan VS, Cheah JH, Clemons PA, Shamji AF, Clish CB, et al. (2014). Regulation of ferroptotic cancer cell death by GPX4. Cell 156, 317–331. 10.1016/j.cell.2013.12.010. [PubMed: 24439385]

Yates MS, Tauchi M, Katsuoka F, Flanders KC, Liby KT, Honda T, Gribble GW, Johnson DA, Johnson JA, Burton NC, et al. (2007). Pharmacodynamic characterization of chemopreventive triterpenoids as exceptionally potent inducers of Nrf2-regulated genes. Mol. Cancer Ther 6, 154–162. 10.1158/1535-7163.MCT-06-0516. [PubMed: 17237276]

Yoo SE, Chen L, Na R, Liu Y, Rios C, Van Remmen H, Richardson A, and Ran Q. (2012). Gpx4 ablation in adult mice results in a lethal phenotype accompanied by neuronal loss in brain. Free Radic. Biol. Med 52, 1820–1827. 10.1016/j.freeradbiomed.2012.02.043. [PubMed: 22401858]

Young MD, and Behjati S. (2020). SoupX removes ambient RNA contamination from droplet-based single-cell RNA sequencing data. GigaScience 9, giaa151. 10.1093/gigascience/giaa151.

Zhu J, Berisa M, Schwörer S, Qin W, Cross JR, and Thompson CB (2019). Transsulfuration activity can support cell growth upon extracellular cysteine limitation. Cell Metab. 30, 865–876.e5, e865. 10.1016/j.cmet.2019.09.009.

Zou Y, and Schreiber SL (2020). Progress in understanding ferroptosis and Challenges in its targeting for therapeutic benefit. Cell Chem. Biol 27, 463–471. 10.1016/j.chembiol.2020.03.015. [PubMed: 32302583]

Highlights

- Female sex confers striking protection against ferroptosis in mouse kidneys
- NRF2 antioxidant pathway is a female resilience mechanism against ferroptosis
- NRF2 controls cell fate and plasticity by regulating ferroptosis
- Female resilience factors can be harnessed to improve kidney injury and repair

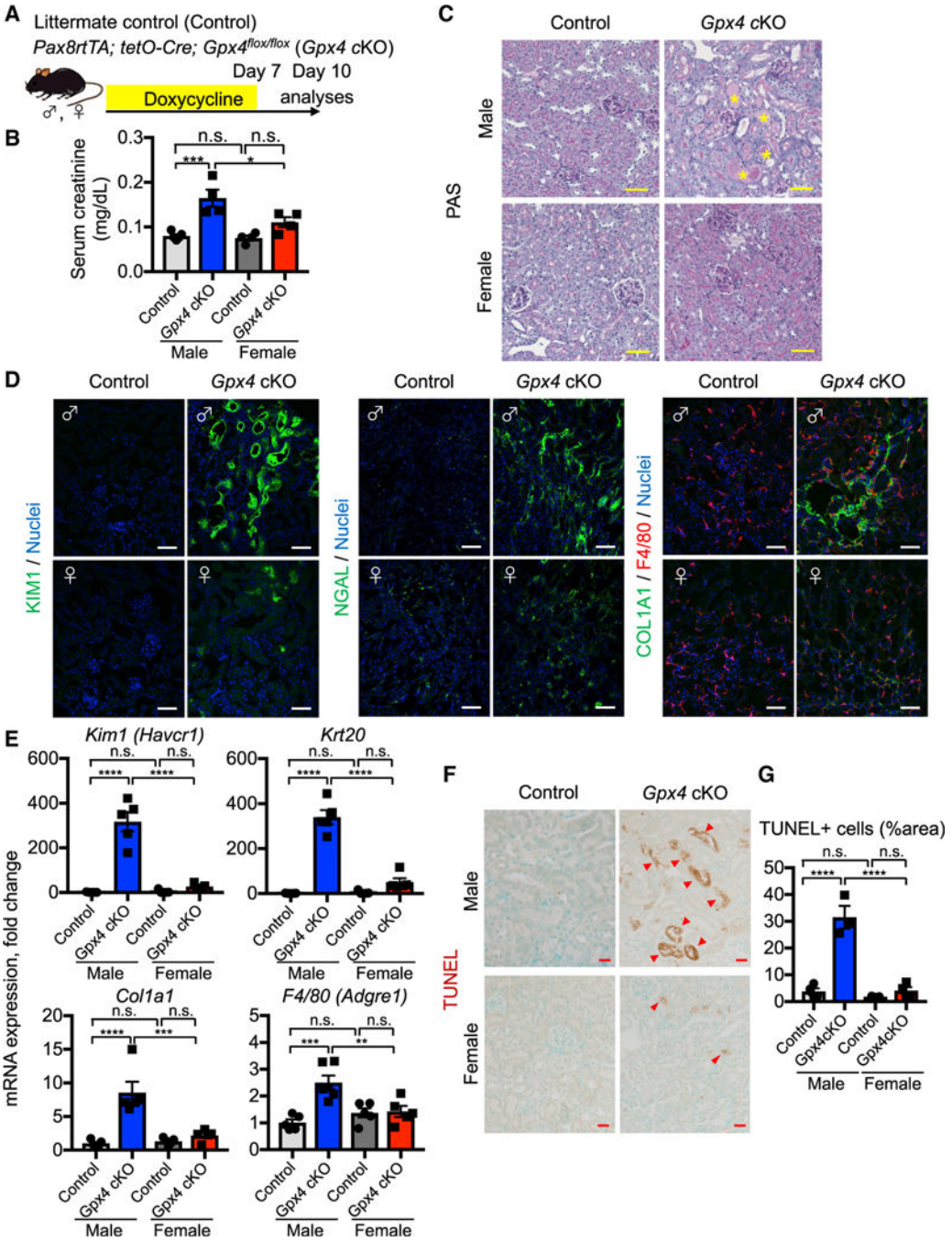

Figure 1. Female kidneys are protected from ferroptosis

(A) Experimental workflow for genetic deletion of *Gpx4*, encoding a canonical anti-ferroptosis enzyme, in renal tubular epithelial cells. Doxycycline was given to control and *Gpx4* cKO mice for 7 days, and kidneys were harvested on day 10.

(B) Serum creatinine levels in control versus *Gpx4* cKO male and female mice. n = 4–5.

(C) Representative images of periodic-acid Schiff (PAS)-stained kidneys. *, hyaline casts. n = 4.

(D) Immunostaining for tubular injury markers (KIM1 and NGAL), macrophages (F4/80), and fibrosis (COL1A1). For quantification, see Figure S1F. n = 4–5.
(E) Real-time PCR analyses of gene expression. n = 5–6.
(F and G) TUNEL staining for evaluating cell death. Quantification of $TUNEL^+$ area is shown in (G) n = 3–4. Arrowheads, $TUNEL^+$ cells. cKO, conditional knockout. One-way ANOVA with post hoc multiple comparisons test. n.s., not significant. *p < 0.05; **p < 0.01; ***p < 0.001; ****p < 0.0001. Scale bars: 50 μm in (C) and (D) and 20 μm in (F). Data are represented as mean ± SEM.
See also Figure S1.

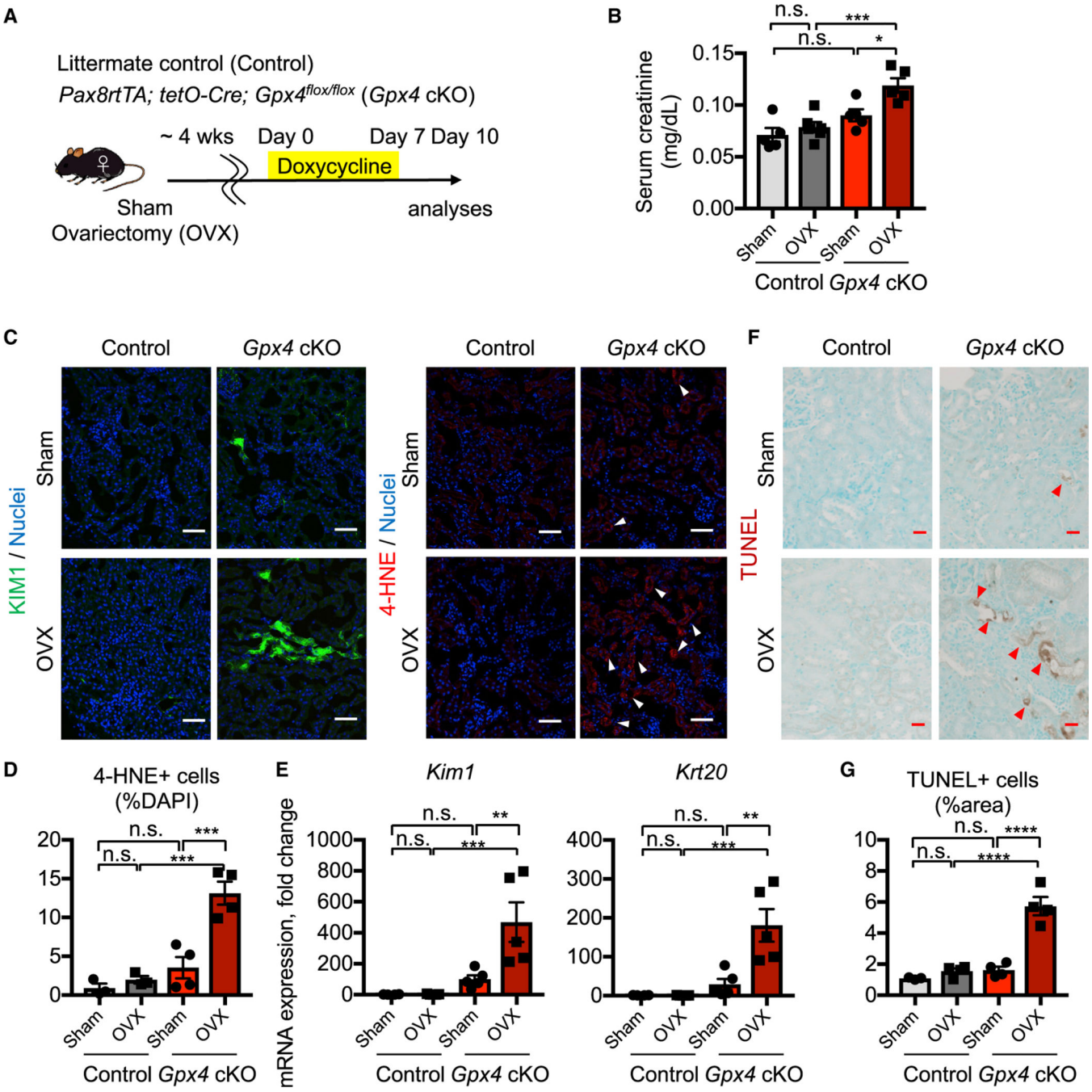

Figure 2. Intact ovarian function underlies female ferroptosis resilience

(A) Experimental workflow for testing ovarian function in female ferroptosis resistance by ovariectomy (OVX). Animals were allowed to recover for 4 weeks after OVX and then treated with doxycycline for 7 days to delete *Gpx4*. Kidneys were harvested on day 10. Control, *Gpx4*-intact control genotype; Sham, sham-operated mice.

(B) Serum creatinine levels. n = 5–6.

(C) Immunostaining for KIM1 (n = 4) and 4-HNE, a toxic lipid peroxide product (n = 3–4). Arrowheads, 4-HNE^{high} cells. For quantification of KIM1, see Figure S2B.

(D) Quantification of 4-HNE$^+$ cells in (C). n = 3–4.
(E) Real-time PCR analyses of indicated gene expression. n = 4–5.
(F and G) TUNEL staining for evaluating cell death. Quantification of TUNEL$^+$ area is shown in (G) n = 3–4. Arrowheads, TUNEL$^+$ cells.
One-way ANOVA with post hoc multiple comparisons test. n.s., not significant. *p < 0.05; **p < 0.01; ***p < 0.001; ****p < 0.0001. Scale bars: 50 μm in (C) and 20 μm in (F). Data are represented as mean ± SEM.
See also Figure S2.

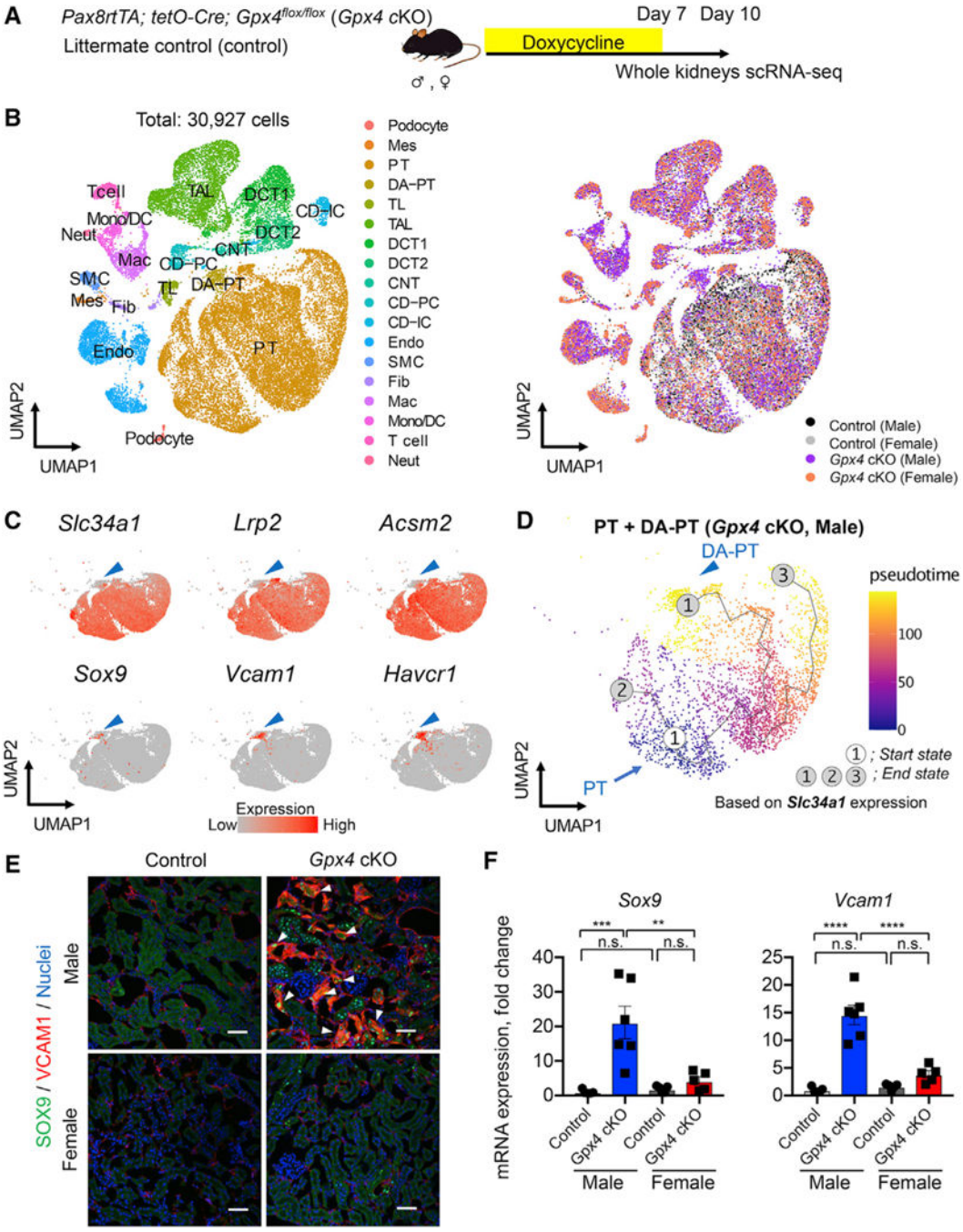

Figure 3. scRNA-seq identifies inflammatory PT cells in male *Gpx4*-deficient kidneys

(A) Experimental workflow for single-cell RNA sequencing (scRNA-seq). Mice were fed with doxycycline-containing water for 7 days, and kidneys were harvested on day 10 to generate scRNA-seq datasets.

(B) Integrated single-cell transcriptome map. Unsupervised clustering identified all major renal cell types in the UMAP plot. PT, proximal tubule; DA-PT, damage-associated PT; TL, thin limb; TAL, thick ascending limb; DCT, distal convoluted tubule; CNT, connecting tubule; CD, collecting duct; PC, principal cells; IC, intercalated cells; Mes, mesangial cells;

Endo, endothelial cells; SMC, smooth muscle cells; Fib, fibroblasts; Mac, macrophages; Mono/DC, monocytes and dendritic cells; Neut, neutrophils.

(C) UMAP plots showing the expression of indicated genes in PT and DA-PT clusters. Differentiated/mature PT cell markers: *Slc34a1* (sodium-dependent phosphate transporter 2a [NaPi2a]), *Lrp2* (megalin), and acyl-coenzyme A synthetase (*Acsm2*), and damage-induced genes: Sry-box 9 (*Sox9*), vascular adhesion molecule 1 (*Vcam1*), and *Havcr1* (*KIM1*). Arrowheads: DA-PT.

(D) Pseudotime trajectory analysis of proximal tubular cells (PT and DA-PT) from male *Gpx4* cKO mice. A region occupied with cells with high *Slc34a1* expression was set as a starting state.

(E) Immunostaining for SOX9 and VCAM1. n = 3. Arrowheads: $SOX9^{+}/VCAM1^{+}$ cells.

(F) Real-time PCR analyses of indicated gene expression. n = 5–6.

One-way ANOVA with post hoc multiple comparisons test. n.s., not significant. **p < 0.01; ***p < 0.001; ****p < 0.0001. Scale bars: 50 μm in (E). Data are represented as mean ± SEM.

See also Figure S3 and Data S1.

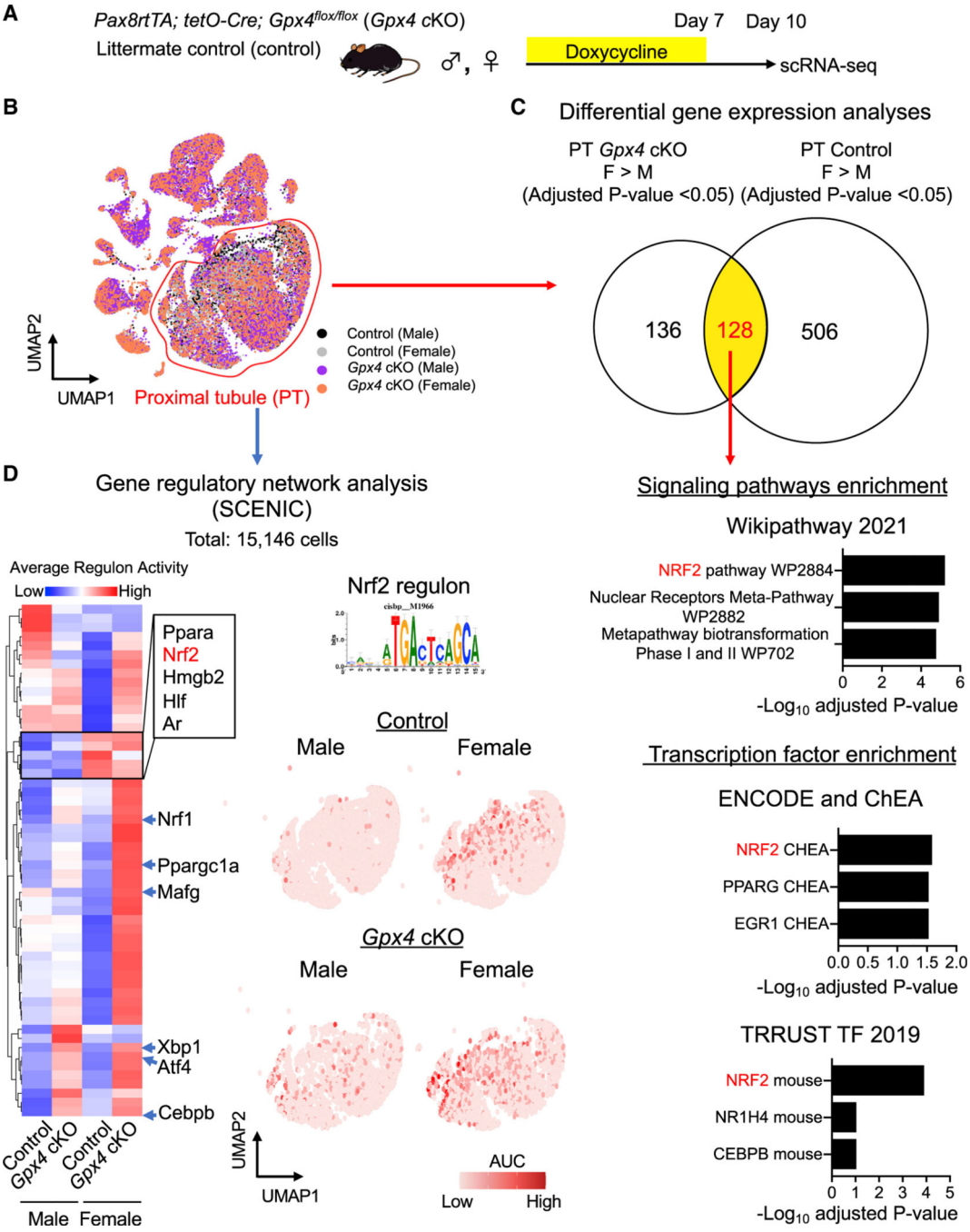

Figure 4. scRNA-seq identifies NRF2 as a mechanism for female ferroptosis resilience

(A and B) Experimental workflow for identifying regulatory nodes underlying sex differences of ferroptosis sensitivity. A total of 15,146 PT cells from all conditions was used for downstream analyses.

(C) Differential gene expression analyses identify 128 genes that are highly expressed in female PT cells compared with male counterparts both at *Gpx4*-intact control and *Gpx4*-knockout conditions. The 128 genes were subjected to Enrichr analysis. Overrepresented signaling pathways and enriched transcription factors are shown.

(D) Single-cell regulatory network inference and clustering (SCENIC) identifies potential nodes that regulate PT cell states in the ferroptotic process. Heatmap of regulons derived from SCENIC is shown. Regulon activity for NFE2-related factor 2 (NRF2; also known as Nfe2l2) antioxidant transcription factor is shown on UMAP of PT cells (red dots represent cells with high NRF2 activity). AUC, enrichment score for the activity of each regulon. See also Figures S4–S8 and Data S2.

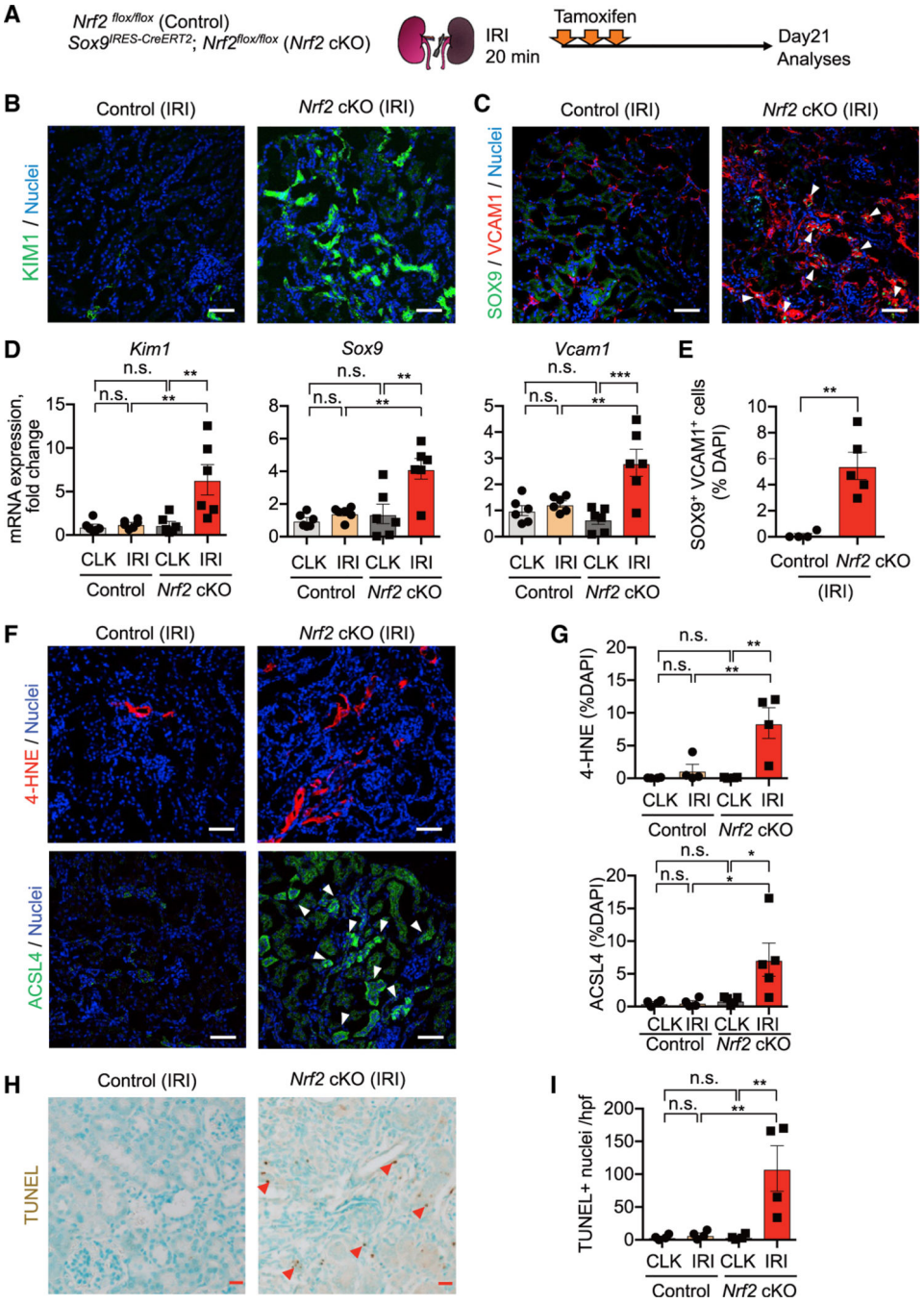

Figure 5. *Nrf2* deletion prevents successful renal repair after IRI

(A) Experimental workflow for testing Nrf2 function in regulating PT cell fate after IRI. *Nrf2* cKO mice and their littermate controls (control) were subjected to the same ischemic stress (20 min) and tamoxifen treatment. *Nrf2* is deleted in *Sox9*-lineage cells after IRI with tamoxifen administration. Kidneys were harvested on day 21 post-IRI.

(B and C) Immunostaining for indicated proteins. Representative images are shown. Arrowheads, $SOX9^+/VCAM1^+$ cells. See Figure S8F for KIM1 quantification.

(D) Real-time PCR analyses of indicated gene expression. n = 6.

(E) Quantification of $SOX9^+/VCAM1^+$ cells (arrowheads in C). n = 4–5.
(F and G) Immunostaining for 4-HNE and ACSL4. Quantifications are shown in (G). n = 4–5. Arrowheads, $ACSL4^+$ cells.
(H and I) TUNEL staining for evaluating cell death. Quantification of $TUNEL^+$ cells is shown in (I). n = 4. Arrowheads, $TUNEL^+$ cells.
One-way ANOVA with post hoc multiple comparisons test for (D), (G), and (I) and t test for (E). n.s., not significant. *$p < 0.05$; **$p < 0.01$; ***$p < 0.001$; ****$p < 0.0001$. Scale bars: 50 μm in (B), (C), and (F) and 20 μm in (H). Data are represented as mean ± SEM.

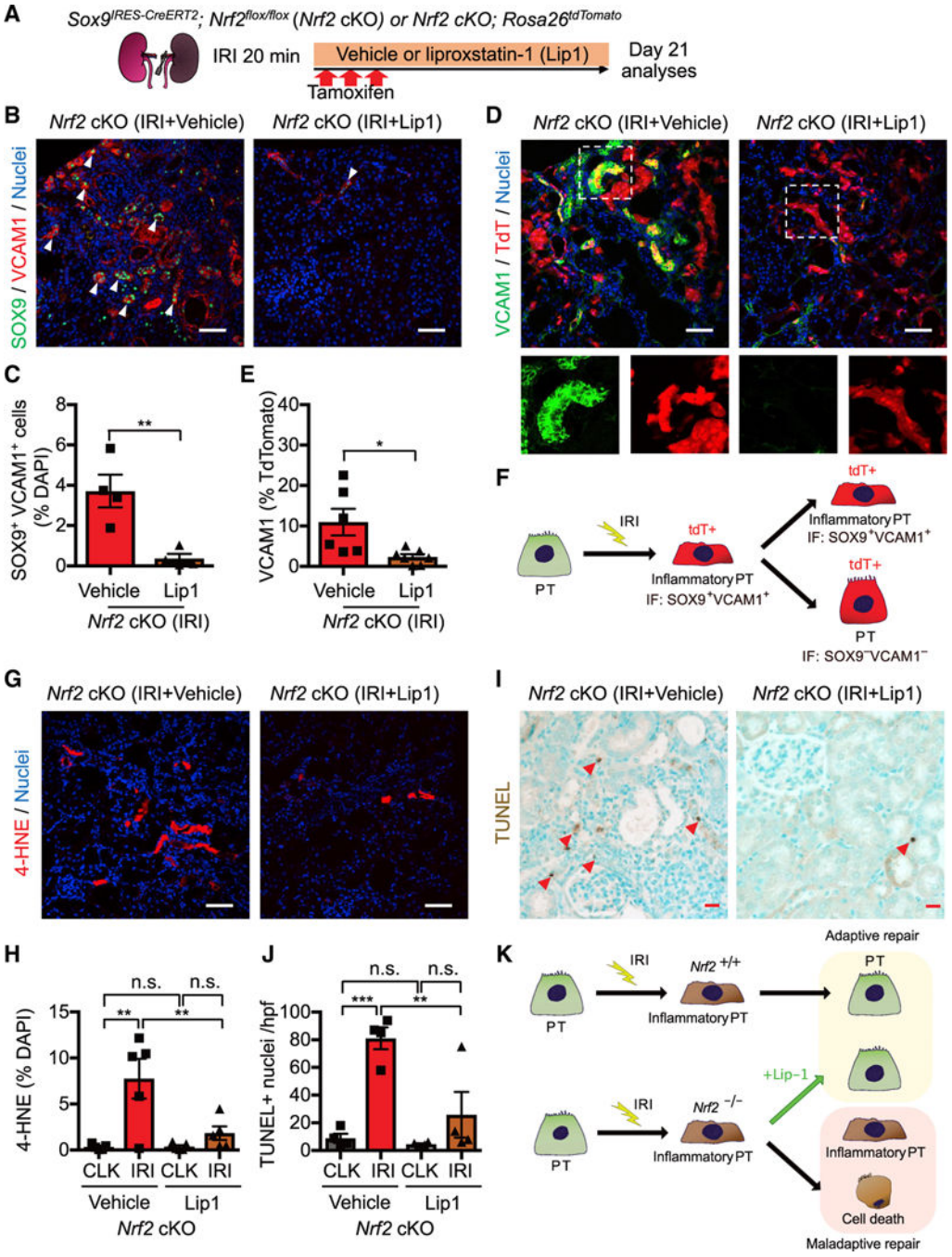

Figure 6. NRF2 governs PT cell fate and plasticity by mitigating ferroptotic stress

(A) Experimental workflow for testing NRF2 function in regulating ferroptotic stress and ferroptosis. *Nrf2* cKO mice were subjected to ischemic stress (20 min) and tamoxifen treatment. The same volume of liproxstatin-1 (Lip-1) or vehicle was intraperitoneally injected daily into the mice. Kidneys were harvested on day 21 post-IRI.

(B and C) Immunostaining for SOX9 and VCAM1. Representative images are shown. Arrowheads, $SOX9^+/VCAM1^+$ cells. Quantification is shown in (C). n = 4.

(D and E) Immunostaining for VCAM1 and fate mapping using tdTomato fluorescence. *Sox9*-lineage cells express tdTomato. Insets: individual fluorescence channels of the dotted box area. Quantification of $VCAM1^+$ cells in *Sox9*-lineage cells is shown in (E). n = 6–7.
(F) Schematic model for PT cell state changes after IRI.
(G and H) Immunostaining for 4-HNE and its quantification. n = 5.
(I and J) TUNEL staining for evaluating cell death. Quantification of $TUNEL^+$ cells is shown in (J). n = 4. Arrowheads, $TUNEL^+$ cells.
(K) Schematic model. Nrf2 regulates PT cell fate by mitigating ferroptotic stress.
Student's t test for (C) and (E) and one-way ANOVA with post hoc multiple comparisons test for (H) and (J). n.s., not significant. *$p < 0.05$; **$p < 0.01$; ***$p < 0.001$; ****$p < 0.0001$. Scale bars: 50 μm in (B), (D), and (G) and 20 μm in (I). Data are represented as mean ± SEM.

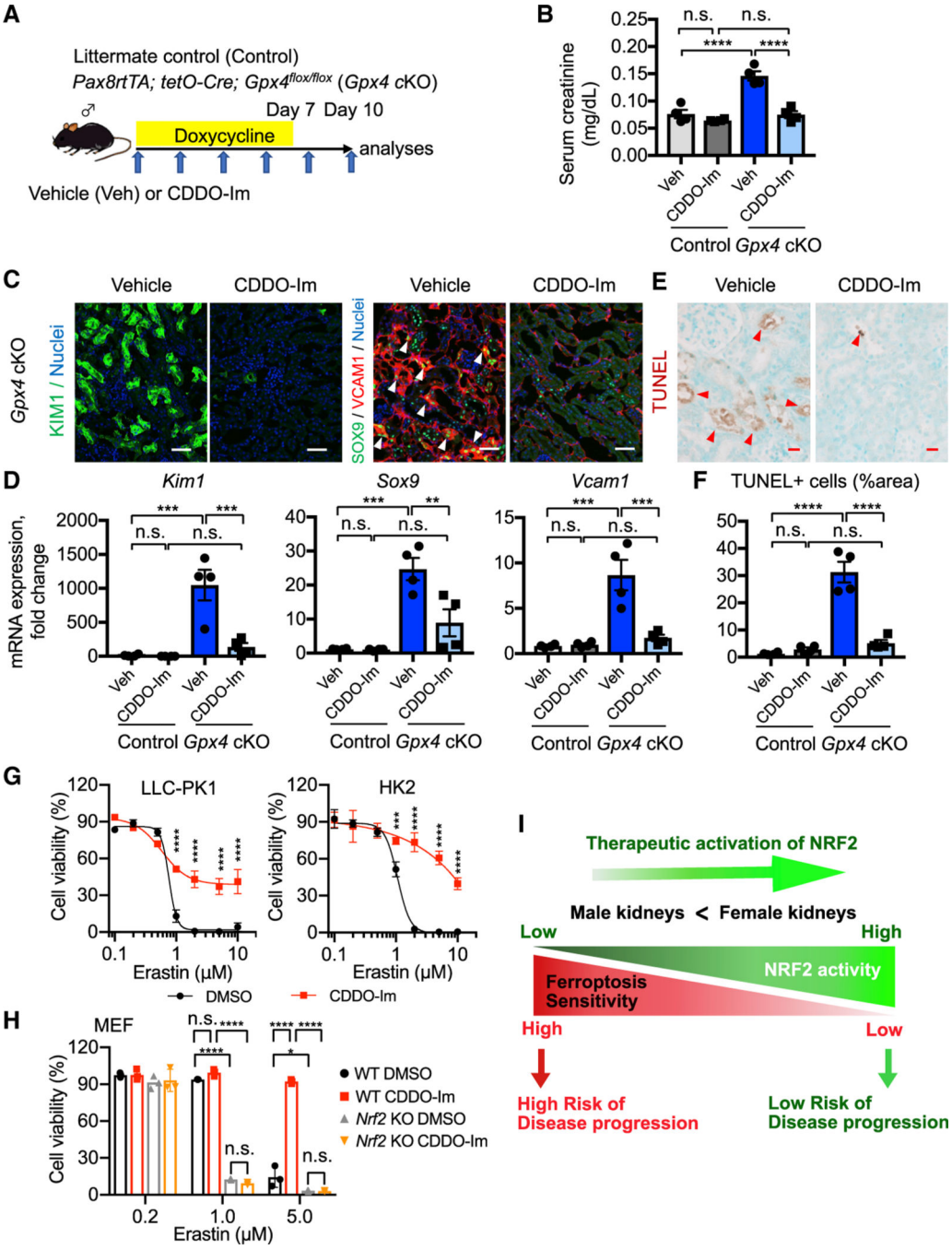

Figure 7. Pharmacological NRF2 activation prevents ferroptosis in *Gpx4*-deficient kidneys

(A) Experimental workflow for testing NRF2 function in regulating ferroptotic stress and ferroptosis using *Gpx4* cKO mice. *Gpx4* cKO mice were administered either vehicle or CDDO-Im (NRF2 inducer) on alternate days. Doxycycline was given for 7 days, and mice were harvested on day 10.

(B) Serum creatinine levels in vehicle- versus CDDO-Im-treated *Gpx4* cKO mice. n = 4.

(C) Immunostaining for KIM1, SOX9, and VCAM1. See Figure S10D for KIM1 quantification. Representative images are shown. Arrowheads, $SOX9^+/VCAM1^+$ cells. n = 4.

(D) Real-time PCR analyses of indicated gene expression. n = 4.

(E and F) TUNEL staining for evaluating cell death. Quantification of $TUNEL^+$ area is shown in (F). n = 4. Arrowheads, $TUNEL^+$ cells.

(G) Cellular viability assays using pig (LLC-PK1) and human (HK2) proximal tubular cell lines.

(H) Cellular viability assays using wild-type (WT) and *Nrf2* knockout mouse embryonic fibroblasts (MEFs). Erastin (system Xc^- inhibitor) was used for inducing ferroptosis in these cells.

One-way ANOVA (B, D, and F) and two-way ANOVA (G and H) with post hoc multiple comparisons test. n.s., not significant. *p < 0.05; **p < 0.01; ***p < 0.001; ****p < 0.0001. Scale bars: 50 μm in (C) and 20 μm in (E). Data are represented as mean ± SEM in (B, D, and F) and mean ± SD in (G and H).

(I) Proposed model. NRF2 acts as a rheostat for modulating ferroptosis sensitivity of proximal tubular cells.

KEY RESOURCES TABLE

REAGENT or RESOURCE	SOURCE	IDENTIFIER
Antibodies		
Goat poiycionai anti-KIM1	R&D Systems	Cat# AF1B17; RRID: AB_2116446
Rat monoclonal anti-NGAL	Abcam	Cat# ab7G2B7; RRID: AB_2136473
Rabbit monoclonal anti-COL1A1	CST	EBF4L; RRID: AB_2904565
Rat monoclonal anti-F4/80	Bio-rad	MCA497; RRID: AB_2098196
Alexa Fluor 488-conjugated Rabbit monoclonal anti-SOX9	Abcam	Cat# ab19645G; RRID: AB_2665383
Rabbit monoclonal anti-SOX9	Abcam	Cat# ab185966; RRID: AB_2728660
Rabbit monoclonal anti-VCAMI	CST	Cat# 39036; RRID: AB_2799146
Alexa Fluor 647-conjugated rabbit monoclonal anti-VCAMI	CST	Cat# 33901; RRID: AB_2799146
Fluorescein-conjugated lotus tetragonolobus lectin (LTL)	Vector	Cat# FL-1321; RRID: AB_2336558
Rabbit polyclonal anti-4-HNE	Abcam	Cat# ab46545; RRID: AB_722490
Rabbit poiycionai anti-Cleaved caspase 3	CST	Cat# 9661; RRID: AB_2341188
Rabbit monoclonal anti-GPX4	Abcam	Cat# ab125066; RRID: AB_10973901
Rabbit monoclonal anti-ACSL4	Abcam	Cat# Ab1552B2; RRID: AB_2714020
Alexa Fluor 488 donkey anti-rabbit	Invitrogen	Cat# A-21206; RRID: AB_2535792
Alexa Fluor 488 donkey anti-goat	Invitrogen	Cat# A-11055; RRID: AB_2534102
Alexa Fluor 488 donkey anti-rat	Invitrogen	Cat# A-21208; RRID: AB_141709
Alexa Fluor 568 donkey anti-rabbit	Invitrogen	Cat# A10042; RRID: AB_2534017
Alexa Fluor 568 donkey anti-goat	Invitrogen	Cat# A-11057; RRID: AB_142581
Alexa Fluor 647 donkey anti-rabbit	Invitrogen	Cat# A-31573; RRID: AB_2536183
Chemicals, peptides, and recombinant proteins		
Doxycycline hyclate	Sigma	Cat# D9891
Tamoxifen	Sigma	Cat# T5648
Peanut oil	Sigma	Cat# 2144
Dimethyl Sulfoxide (DMSO), sterile filtered	Sigma	Cat# D2438
Liproxstatin-1	Selleckchem	Cat# S7699
CDDO-Im	Tocris	Cat# 47-371-0

REAGENT or RESOURCE	SOURCE	IDENTIFIER
Kolliphor EL	Sigma	Cat# C5135
Liberase TM	Roche	Cat# 291963
Hyaluronidase	Sigma	Cat# H4272
DNasel	Roche	Cat# 11284932001
Trypsin EDTA 0.25%	Corning	Cat# 25-052-CI
Fetal bovine serum	Corning	Cat# 35-010-CV
PBS	Corning	Cat# 21-040-CV
Bovine serum albumin	VWR	Cat# 97061-416
Trizol	Invitrogen	Cat# 15596026
Maxima H minus cDNA synthesis master mix	Invitrogen	Cat# M1662
PoswerUp SYBR Green Master Mix	Invitrogen	Cat# A25776
Animal free blocker	Vector	Cat# SP-5030
TrueVIEW autofluorescence quenching kit	Vector	Cat# SP-8400
LPS, E. Coli serotype O111:B4	Sigma	Cat# L2630
DMEM high glucose	Corning	Cat# 10-017-CV
Penicillin Streptomycin	Corning	Cat# 30-002-CI
IMDM	Thermo	Cat# 76050
Primocin	Invitrogen	Cat# ANT-PM-1
Erastin	Tocris	Cat# 5449
IHC antigen retrieval solution	Invitrogen	Cat# 00-4955-58
PrestoBlue viability reagent	Invitrogen	Cat# A13262
Critical commercial assays		
1Gx Chromium Single Ceil 3’ Reagent kit v3.1	10x Genomics	Cat# PN-1000268
TUNEL staining kit	Abcam	Cat# ab206386
ImmPRES HRP reagent kit	Vector	Cat# MP-7401
PAS staining kit	Sigma	Cat# 395B
RNAScope Multiplex Fluorescent Reagent Kit v.2	ACD	Cat# 323100
RNA Protein Co Detection kit	ACD	Cat# 323180
RNAScope probe: Mm-*Gsfa4*	ACD	Cat# 1132411
RNAScope probe: Mm-*Gstm1*	ACD	Cat# 503461

REAGENT or RESOURCE	SOURCE	IDENTIFIER
RNAScope probe: Mm-*Mgst1*	ACD	Cat# 861961
Deposited data		
scRNA-sequencing for Gpx4-deleted kidneys	This paper	GEO: GSE197528
scRNA-sequencing for ischemia-reperfusion-injured kidneys	Ide et ai., eLife 2021	GEO: GSE161201
Experimental models: Ceil lines		
HK2	ATCC	CRL-2190
LLC-PK1	ATCC	CL-101
MEF (wild type)	Wakabayashi et ai. 2010	N/A
MEF (Nrf2 knockout)	Wakabayashi et ai. 2010	N/A
Experimental models: Organisms/strains		
Mouse: *PaxSrtTA*: B6.Cg-Tg(PaxB-rtTA2S*M2)1Koes/J	Traykova-Brauch, et ai., 2008	Jackson Laboratory: Stock# 007176
Mouse: *tetO-Cre*: B6.Cg-Tg(tetO-cre)1Jaw/J	Perl, et al., 2002	Jackson Laboratory: Stock# 006234
Mouse: $Gpx4^{flox}$: $Gpx4^{tm1.1Qra}$/J	Yoo et al. 2012	Jackson Laboratory: Stock# 027964
Mouse: $Nrf2^{flox}$: C57BL/6-$Nfe2/2^{tm1.1Sred}$/SbisJ	Kong et al. 2011	Jackson Laboratory: Stock# 025433
Mouse: $Rosa26^{tdTomato}$: B6. Cg-$Gt(ROSA)26Sor^{tm14(CAG-tdTomato)Hze}$/J	Madisen et al. 2010	Jackson Laboratory: Stock# 007914
Mouse: $Sox9^{IRES-CreERT2}$: $Sox9^{tm1(cre/ERT2)Haak}$	Soeda et al. 2010	RRID:MGI:4947115
Oligonucleotides		
See Table S1 for genotyping primers		
See Table S2 for real-time quantitative PCR primers		
Software and algorithms		
10x Chromium Cell Ranger ver. 6.0.1	10x Genomics	https://support.1Gxgenomics.com/single-cell-gene-expression/software/pipelines/latest/what-is-cell-ranger
Seurat v.4.06	Hao et al. 2021	https://satijaiab.org/seurat/
DoubletFinder (ver. 2.03)	McGinnis et al. 2019	https://github.com/chris-mcginnis-ucsf/DoubletFinder
SoupX (ver. 1.5.2)	Young and Behjati 2020	https://github.com/constantAmateur/SoupX
SCTransform	Hafemeister and Satija 2019	https://satijaiab.org/seurat/articles/sctransform_vignette.html

REAGENT or RESOURCE	SOURCE	IDENTIFIER
EnhancedVolcano v1.10.0	N/A	https://bioconductor.org/packages/release/bioc/html/EnhancedVolcano.html
Monocle 3 (version 1.0.0)	Cao et al., 2019	https://coie-trapneii-iab.github.io/monocie3/
Enrichr	Kuleshov et al. (2016)	https://maayanlab.doud/Enrichr/
SCENIC (ver.1.2.4)	Aibar et al. (2017)	https://scenic.aertsiab.org/
ImageJ	NIH	https://imagej.nih.gov/ij/
GraphPad Prism	Graph Pad	https://www.graphpad.com/
Kidney Cell Explorer	Ransick et al. 2019	https://ceiio.shinyapps.io/kidneyceiiexpiorer/